

Constraints on the deformation and rupturing of continental lithosphere of the Red Sea: the transition from rifting to drifting

J. R. COCHRAN¹ & G. D. KARNER²

¹Lamont-Doherty Earth Observatory, Palisades, NY 10964, USA

(e-mail: jrc@ldeo.columbia.edu)

²Present address: ExxonMobil Upstream Research Company, Mail Stop URC-URC-S169A, P.O. Box 2189, Houston, TX, 77252-2189, USA

Abstract: The Red Sea is an ideal locale for testing differing models and hypotheses for rift evolution and the initiation of sea-floor spreading. The Red Sea is an active rift system that formed by the rifting of Precambrian continental lithosphere beginning in the late Oligocene, leading to breakup and sea-floor spreading by approximately 5 Ma in the southern Red Sea to the south of about 19°30'N. In the northern Red Sea, north of approximately 23°30'N, organized sea-floor spreading is not observed, although individual volcanoes are located within discrete 'deeps' spaced along the axial depression. These have been interpreted as marking the beginning of a transition from amagmatic, mechanical rifting to magmatic, oceanic spreading. Based on seismic reflection and refraction, gravity, magnetic and heat flow data in the northern Red Sea, it has been suggested that rift development occurs via the rotation of large crustal fault blocks that sole into a zone of plastic creep in the lower crust, resulting in a flat Moho and high upper crustal relief. Melt formed within individual rift segments is focused to form small axial volcanoes. That is, the northern Red Sea is on the verge of replacing horizontal translation with focused mantle upwelling and organized sea-floor spreading. In marked contrast, many passive margins (e.g. West Africa, Brazil, and NW and NE Australia) are characterized by the stacking of regional synrift sag packages, the thickness and distribution of which are inconsistent with the minor amounts of brittle deformation mapped from seismic sections. A fundamental implication of this observation is that rifts characterized by large offset fault systems, (i.e. faults that generate synrift accommodation, such as in the Basin and Range province and East Africa) will not proceed to breakup. The challenge is to understand why different portions of the Red Sea show different stages in the development of a spreading centre during continental rifting. Two hypotheses exist: (1) the structural framework deduced in the north simply continues to the south where sea-floor spreading exists and that the two regions are registering a difference in total extension. Thus, the northern Red Sea has experienced insufficient extension to breach the continental lithosphere but, in time, should develop into a spreading centre; or (2) the lithosphere of the northern Red Sea region is rheologically stronger compared with the lithosphere of the southern Red Sea, perhaps as a consequence of the thermal effects of the Afar plume, and the northern Red Sea will never evolve to sea-floor spreading. The existence of large rotated fault blocks, as implied from the inversion of gravity and magnetic anomaly data, favours the latter.

Exactly how the lithosphere ruptures to form a rifted continental margin and a new ocean basin (i.e. the transition from extension to sea-floor spreading), and why some rifts succeed in making this transition while others fail, is poorly known. The Red Sea is an ideal locale for testing differing models and hypotheses for rift evolution and the initiation of sea-floor spreading. The Red Sea is an active rift system that formed by the rifting of Precambrian continental lithosphere beginning in the late Oligocene, leading to breakup and sea-floor spreading by about 5 Ma in the southern Red Sea to the south of approximately 19°30'N (Roeser 1975). In the northern Red Sea, north of approximately 23°30'N, organized sea-floor spreading is not observed, although individual volcanoes are located within discrete 'deeps' spaced along the axial

depression. These have been interpreted as marking the beginning of a transition from amagmatic, mechanical rifting to magmatic, oceanic spreading (Pautot *et al.* 1986; Martinez & Cochran 1988; Cochran 2005). Between these two regions (in the central Red Sea) there is a transition area where sea-floor spreading cells have nucleated, but have not linked to form a continuous axis (Pautot 1983; Cochran 1983; Bonatti 1985; Bicknell *et al.* 1986). A fundamental question is whether sea-floor spreading is propagating from south to north or whether the mode of extension in the northern Red Sea has in some way prevented the development of sea-floor spreading in that region.

Based on data in the northern Red Sea, Cochran (2005) suggested that rift development occurs via the rotation of large crustal fault blocks that sole

into a zone of plastic creep in the lower crust, resulting in a flat Moho and high upper crustal relief. Initial broadly distributed extension is eventually replaced by focused extension at the rift axis leading to rapid lithospheric thinning and melt generation. Melt formed within individual rift segments is focused to form small axial volcanoes (Cochran 2005). With continued extension and magmatism, these volcanoes may become cells of sea-floor spreading that grow and coalesce to form a continuous axis, as exists in the southern Red Sea. That is, the northern Red Sea is on the verge of replacing horizontal translation by focused mantle upwelling and organized sea-floor spreading.

Given that considerably more extension has occurred in the southern than in the northern Red Sea, as determined by the difference in opening rate between Arabia and Nubia (Roeser 1975; Joffe & Garfunkel 1987; Chu & Gordon 1998; Jestin *et al.* 1998), then why even question that sea-floor spreading will simply propagate northwards into the northern Red Sea? Karner *et al.* (2003) and Karner (2005) have shown that the West African, Brazilian and NW Australian passive continental margins are characterized by the stacking of regional synrift sag basins, the amplitude and distribution of which are inconsistent with the minor amounts of brittle deformation mapped from seismic sections. The sag basins exhibit none of the diagnostic features expected of synrift extensional systems (e.g. normal faults that control accommodation, rotation of crustal blocks, prominent rift onset unconformities, synrift sediment wedges). While the South Atlantic margins do show a number of large, late-rift stage faults, these faults generally fail to explain the regional development of synrift accommodation across the region and are thus relatively unimportant in the extension process. The fundamental implication of this model is that rifts characterized by large normal fault systems controlling synrift accommodation, such as in the Basin and Range province, East African rift system, North Sea Basins, Rhine-graben and Newark Basin, will not proceed to breakup. By analogy, because of the existence of large fault blocks in the northern Red Sea, the implication is that it should never proceed to sea-floor spreading. The challenge is to understand why different portions of the Red Sea show different stages in the development of a spreading centre during continental rifting.

Cochran (2005) based his model on data from the northern Red Sea and assumes that the structural framework deduced in the north continues to the south where sea-floor spreading exists. However, it is entirely conceivable that the two areas, separated by a major tectonic boundary (the 'Zabargad fracture zone' Crane & Bonatti 1987), have

developed differently and observations in the northern Red Sea cannot be extrapolated to the south where few data are available for comparison. Thus, the difference between the two regions may be owing to a fundamental difference in lithosphere rheology, explaining why sea-floor spreading developed in the southern, but not the northern, Red Sea. The counter-argument is that the entire Red Sea is developing similarly, but rifting in the northern and central Red Sea simply has experienced insufficient extension to develop into sea-floor spreading at this time.

In this paper, we will compare and contrast the two models presented above by using existing geophysical data from the region to understand why different portions of the Red Sea show different stages in the development of a spreading centre within a continental rift. For a combination of logistic and political reasons, most of the available geophysical data are concentrated in the northern Red Sea. The morphology and other geophysical parameters for much of the central and southern Red Sea are only known in general terms with Backer *et al.*'s (1975) single-beam sonar survey still the primary data source. First, we briefly review the prerift development of the Red Sea area and how the pre-existing structure influenced the form and distribution of rifting and the influence of the Afar plume. Finally, we will discuss the structure of the northern and central Red Sea and develop a model for how possible differences between these two areas may influence the future development of the Red Sea.

Prerift constraints

The Red Sea rift propagates through the late Precambrian (Pan-African) Afro-Arabian shield. The basement rocks exposed on the adjacent rift shoulders consist of a variety of granitic, metamorphic, and mafic igneous rocks comprising a number of different terrains separated by suture zones and interpreted as a series of collapsed and accreted island arcs that were assembled between 900 and 600 Ma (e.g. Camp 1984; Stoeser & Camp 1985; Vail 1985; Kroner *et al.* 1991). Two nearly north-south-trending late Precambrian suture zones within the Pan-African lithosphere, the Baraka and Onib-Hamisana sutures, intersect the Red Sea Rift near 18°N and 22°N, respectively. At both locations there are pronounced kinks in the overall N30°E trend of the rift and a corresponding offset of the rift axis (Dixon *et al.* 1987; Crane & Bonatti 1987; Bosworth *et al.* 2005) (Fig. 1).

The hinge zone of the Mediterranean margin is located just to the north of the Gulf of Suez (Steckler & ten Brink 1986). A change in Eurasian–African plate motions in the late Santonian resulted

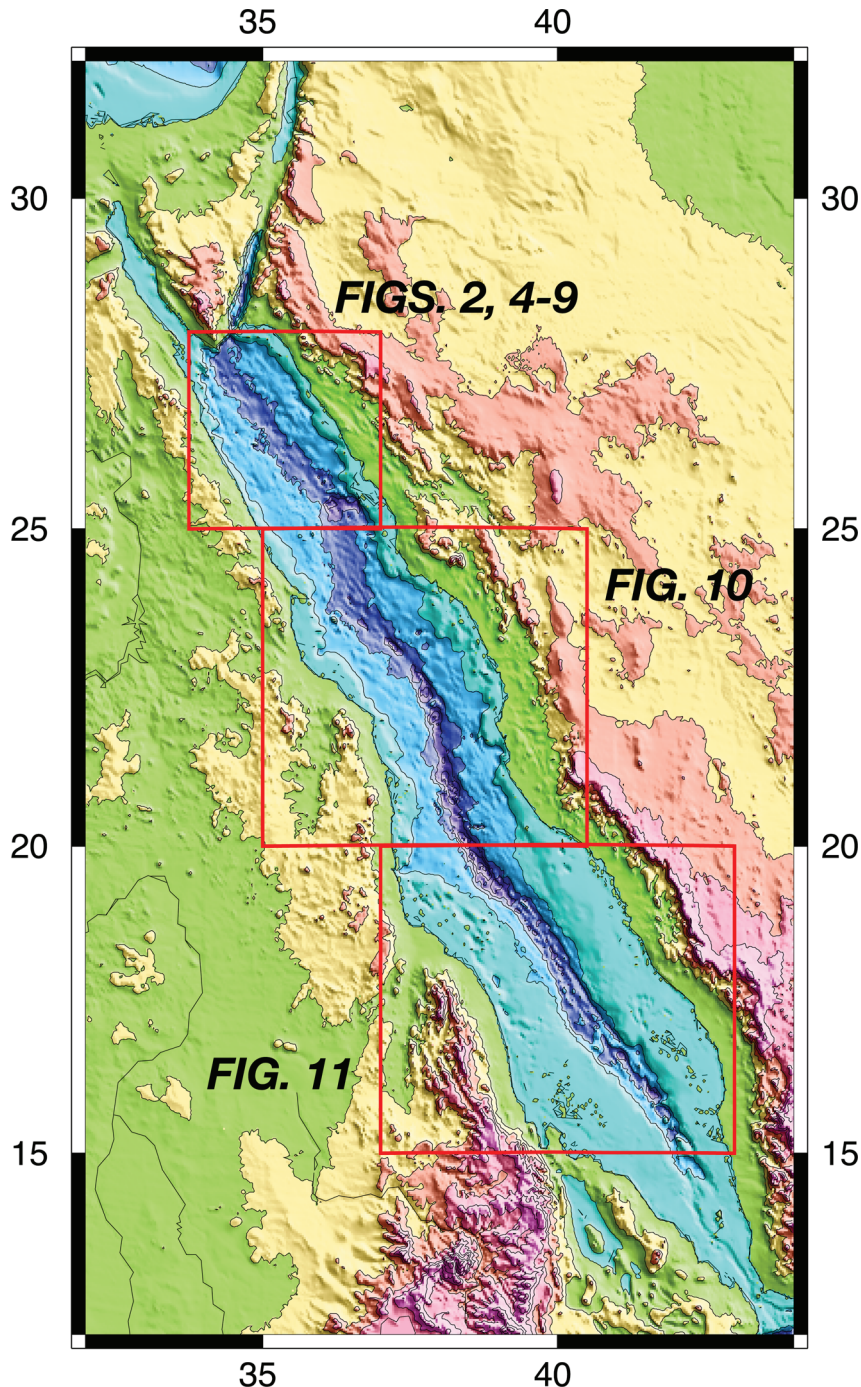


Fig. 1. Red Sea location map. Bathymetry and topography are from Smith & Sandwell (1997), contoured at 500 m intervals. The maps shown in Figures 2 and 4–9 are of the northern region and are outlined in red. The location of Figure 11 and 12 of the central and southern Red Sea region are also outlined in red. All images of data grids assume an artificial shadowing from the NE.

in transpressional deformation and the development of 'Syrian Arc' structures along the Mediterranean margin (Moustafa & Khalil 1990; Guiraud & Bosworth 1997, 1999; Guiraud *et al.* 2005) with more minor deformation occurring farther south in the region of the future Gulf of Suez and northern Red Sea (Bosworth *et al.* 1999). These structures were reactivated, again in transpression, in the late Eocene (Moustafa & Khalil 1994; Guiraud *et al.* 2001, 2005).

The combination of the Syrian Arc structures and the transition from continental to stronger oceanic lithosphere defined the nature and location of the northern termination of the Red Sea rift. Upon reaching the main Syrian Arc deformation, Red Sea rift extension, which had been confined to a reasonably narrow rift, spread out over a broad region from the Bitter Lakes west to Cairo (Bosworth & McClay 2001; Bosworth *et al.* 2005). The Manzala Rift continues north from Cairo under the Nile Delta (Bosworth & McClay 2001), but does not appear to penetrate far into oceanic Mediterranean lithosphere. Later in the mid-Miocene, the Dead Sea rift developed in continental lithosphere just landward of the Mediterranean hinge zone (Steckler & ten Brink 1986), more or less cutting off the Gulf of Suez.

A series of rifts, apparently related to rifting between Africa and India/Madagascar developed in the late Jurassic and early Cretaceous across the Horn of Africa and extended into Yemen and Somalia (Bott *et al.* 1992; Redfern & Jones 1995; Ellis *et al.* 1996; Brannan *et al.* 1997). Further south, the similar age Anza Rift extends from the Kenyan continental margin into SE Sudan where there are a series of NW–SE-trending Late Jurassic rifts referred to as the Central African rift system (Bosworth 1992). Later in the Cretaceous (Barremian–Albian) more northern portions of Sudan, as well as the Sirte Basin in Libya and Abu Ghadiq Basin in the western Desert of Egypt, were subjected to extensional deformation (Bayoumi & Lofty 1989; Guiraud & Maurin 1992; Guiraud 1998).

These extensional tectonic events did not extend across the future location of the Red Sea rift and do not appear to have had a significant impact on the lithosphere thickness and thermal structure. Heat flow measurements in Egypt at distances of more than about 30 km from the present Red Sea rift are in the range of 35–55 mW m⁻² (Morgan *et al.* 1985; Boulos 1990), consistent with a stable tectonic regime and thick lithosphere. The few published heat flow measurements from the Arabian portion of the shield are also in the range of 35–45 mW m⁻² (Gettings 1982; Gettings & Showail 1982; Gettings *et al.* 1986).

Information on the crustal and lithospheric thickness and structure is limited. Knopoff &

Fouda (1975) utilized Raleigh wave dispersion to deduce a crustal thickness of about 37 km beneath Arabia. Their results also show a pronounced low-velocity layer, the top of which is at a depth of 100–140 km. The US Geological Survey acquired a 1000 km-long seismic refraction profile across Arabia from near Riyadh to the Farasan Islands at 16°N in the southern Red Sea (Healy *et al.* 1982); crustal thickness was estimated to be in the range of 37–45 km away from the Red Sea rift. The crust appears to thin by about 5 km approaching the rift, the crust consisting of two layers, each layer being about 20 km thick. The average velocities of the two layers are 6.3 and 7.0 km s⁻¹. The crust–mantle boundary appears to be transitional over a distance of 2–8 km and the mantle velocity is in the range of 8.0–8.2 km s⁻¹.

Makris *et al.* (1979, 1983) and Rihm *et al.* (1991) presented three seismic transects extending inland for about 150 km from the coast in the northern Red Sea. The transect on the Arabian side, at 26°N, was interpreted as showing a 40 km-thick crust at distances greater than about 100 km from the coast with a gradual decrease in crustal thickness toward the rift (Makris *et al.* 1983). The two lines on the African side, at 27°N and 26°N, show a thinner 30–35 km-thick crust away from the rift and a much more abrupt thinning of the crust approaching the Red Sea (Makris *et al.* 1979; Rihm *et al.* 1991), although neither of these seismic lines are reversed.

Initiation of rifting

The onset of rifting in the Red Sea was preceded by massive volcanism in Ethiopia and southern Yemen (e.g. Mohr 1983). Based on stratigraphic relationships and ⁴⁰Ar/³⁹Ar dating, the majority of the basalts were erupted over a short (*c.* 1.5 Ma) time period at approximately 30 Ma (Baker *et al.* 1996; Hofmann *et al.* 1997; Coulie *et al.* 2003), although activity continued to about 25 Ma (Ukstins *et al.* 2002). Rhyolitic volcanism began at about the same time and continued until about 26.5 Ma (Baker *et al.* 1996). This short burst of flood volcanism has been attributed to impingement of the Afar plume head on the lithosphere (e.g. Richards *et al.* 1989). Bosworth *et al.* (2005) emphasize the observation that the extensive volcanism from 31 to 25 Ma was not associated with significant extension.

Although the massive approximately 30 Ma volcanism was centred in Ethiopia and southern Yemen, coeval basalt flows have been reported as far north as about 18°N in Sudan. Drury *et al.* (1994) describe basaltic flows reaching a thickness of 600 m that were extruded onto a well-developed laterite palaeosol in northern Eritrea. Dating of

these flows using $^{40}\text{Ar}/^{39}\text{Ar}$ techniques gave ages of between 32.9 and 28 Ma. Further north, Kenea *et al.* (2001) describe basalt flows overlain by rhyolite from the Odi and Adar Ribad basins of the Derudeb region of eastern Sudan. $^{40}\text{Ar}/^{39}\text{Ar}$ dating of the volcanics shows that they were erupted over a short period from about 31 to 29 Ma. In both regions, stratigraphic relations indicate that extension and uplift related to Red Sea rifting post-dates the volcanism (Drury *et al.* 1994; Kenea *et al.* 2001). Late Oligocene volcanism has not been reported from farther north in northern Sudan or Egypt.

An episode of dyke intrusion (Blank 1977) dated at 24–21 Ma on the basis of K–Ar and $^{40}\text{Ar}/^{39}\text{Ar}$ data is recorded along the entire length of the Red Sea on the Arabian margin (Bartov *et al.* 1980; Eyal *et al.* 1981; Feraud *et al.* 1991; Sebai *et al.* 1991). This episode was more intense in the southern Red Sea, being accompanied in places by intrusion of plutonic bodies of granitic–gabbroic composition (Pallister 1987; Sebai *et al.* 1991; Davison *et al.* 1994). This event extends for a distance of 1700 km along the trend of the Red Sea with no discernable temporal pattern (Sebai *et al.* 1991; Bosworth *et al.* 2005). Although episodic volcanism has continued to the present in Afar and in southern Yemen (e.g. Zumbo *et al.* 1995a, b; Coulie *et al.* 2003), there has been little significant volcanism within the Red Sea rift since the Early Miocene dyking event (Coleman *et al.* 1983; Coleman 1984; Coleman & McGuire 1988; Sebai *et al.* 1991).

The Early Miocene dyke event appears to mark the initiation of extensional rifting in the Red Sea. Bosworth *et al.* (2005) documented the earliest definitive synrift sediments along the length of the Red Sea, which consistently fell in the range of 21–24 Ma. Fission track data from Egypt (Omar *et al.* 1989; Omar & Steckler 1995), SW Saudi Arabia (Bohannon *et al.* 1989) and Eritrea (Abbate *et al.* 2002; Ghebreab *et al.* 2002) also consistently give 21–24 Ma for the onset of significant denudation (and, thus, by inference, rift flank uplift). Omar & Steckler (1995) also suggest a pulse of uplift at about 34 Ma, but there is no dated sedimentary evidence of significant uplift and erosion at this time (Bosworth *et al.* 1998). Bosworth *et al.* (2005) suggest that this event may be related to Syrian Arc tectonics.

Morphology and structure of the northern Red Sea

The Red Sea consists of narrow continental shelves and a broad ‘main trough’ at a depth of 400–1200 m. The shelf broadens in the central Red Sea, and in the southern Red Sea the shelf consists of coral reefs that completely choke the main trough.

From 15°N to 19°30'N in the southern Red Sea, the main trough is cut by an ‘axial trough’ reaching depths of over 2000 m and floored by oceanic basalt formed at a well-developed mid-ocean ridge spreading centre (Roeser 1975; Cochran 1983; Miller *et al.* 1985; Garfunkel *et al.* 1987). The spreading centre becomes discontinuous north of 19°30'N and, with the possible exception of the Mabahiss Deep pull-apart basin centred at 25°20'N, 36°10'E, there is no evidence of oceanic crust north of about 23°N.

The continental margins of the northern Red Sea consist of steep, faulted scarps with 400–1000 m of relief that truncate the narrow continental shelves (Fig. 2) and appear to mark the edge of the actively extending rift. Rotated basement fault blocks forming elongated hills and ridges are found 2–10 km inland from the coast. Mid-Miocene reef platforms are consistently found at an elevation of 200–300 m mantling the seaward edges of these basement fault blocks along both the African (Bosworth *et al.* 1998) and Arabian (Purser & Hötzl 1988) margins. These fault blocks are inactive and have been marked by uplift and non-deposition since the late Miocene (Montentat *et al.* 1988). Mid-Pleistocene reef terraces that have been uplifted 20–50 m are consistently found between the exposed basement fault blocks and the coast. This pattern of uplifted reefs and fault blocks documents a progressive narrowing of the actively extending rift as fault blocks become inactive and are transferred to the uplifting rift flanks.

The bathymetry of the active, main trough of the northern Red Sea rift consists of a series of terraces stepping down to an axial depression at a depth of 1100–1200 m (Martinez & Cochran 1988; Cochran 2005). The terraced nature of the bathymetry is clear on the bathymetry profiles shown in Figure 3.

Sediment deformation within the axial depression is much more intense than in the remainder of the Red Sea (Knott *et al.* 1966; Guennoc *et al.* 1988; Martinez & Cochran 1988), implying that tectonic activity and extension is presently concentrated predominantly in the axial depression. However, the slopes separating terraces often appear to be faulted (Cochran 2005). Also, although earthquakes with $M_L > 3$ are concentrated in the axial depression, smaller earthquakes are distributed throughout the northern Red Sea (Badawy 2005). These two observations imply that some extension still occurs within the main trough away from the axial depression.

Free-air gravity anomaly highs are located on the seaward edges of the terraces on Figure 3. This is a systematic observation throughout the northern Red Sea (Martinez & Cochran 1988; Cochran 2005). Martinez & Cochran (1988) argue that the density anomalies responsible for the

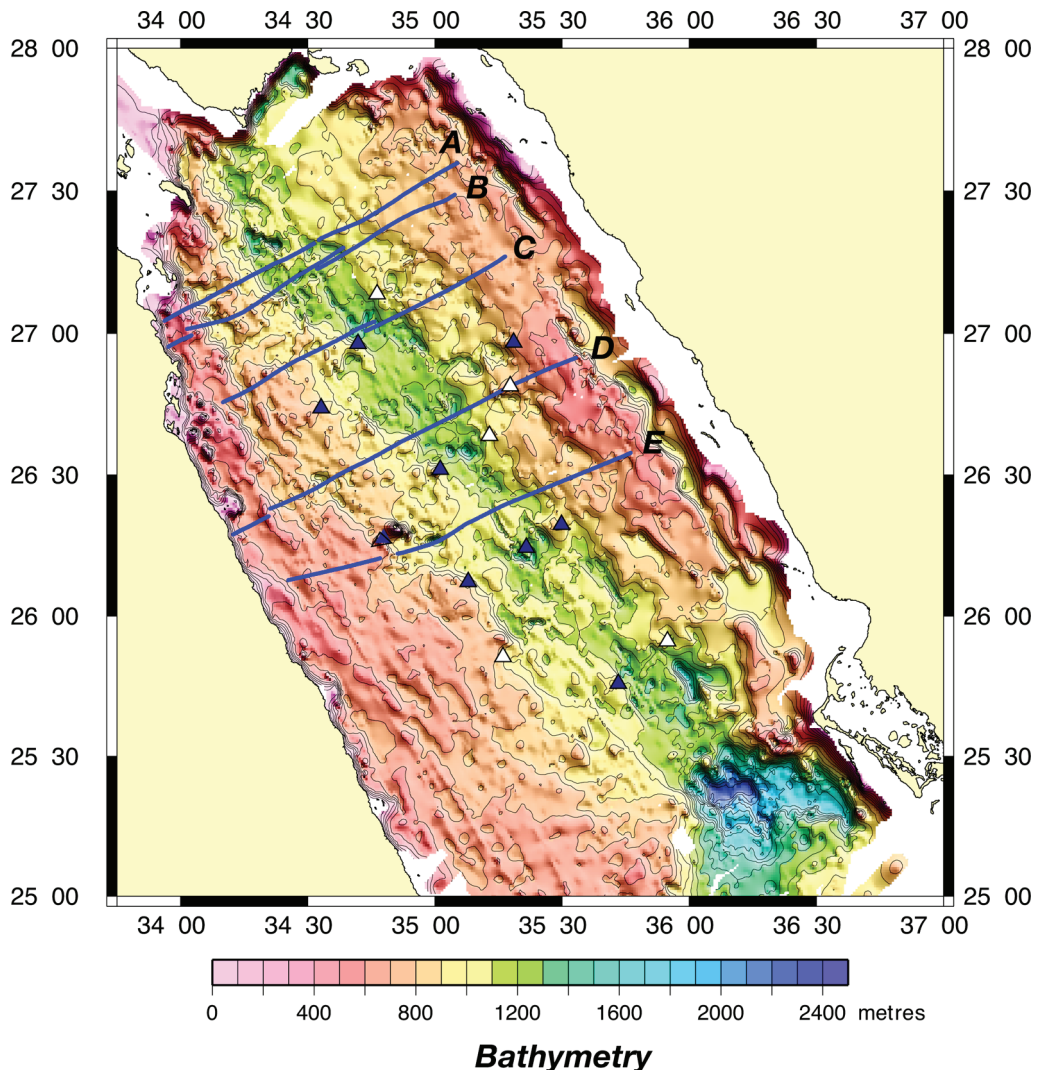


Fig. 2. Northern Red Sea bathymetry map contoured at 100 m-intervals. Data sources for the bathymetry are discussed by Cochran (2005). Projected shipboard bathymetry, gravity and magnetic data profiles used in the Parker and Werner inversions are shown as blue lines (labelled A–E). Triangles mark location of volcanoes identified from the magnetic anomalies. Triangles are blue when the identification is confirmed by bathymetry and/or gravity data and white when based only on interpretation of the magnetic data.

gravity anomalies are sufficiently large to reflect basement relief. As free-air gravity anomalies in the northern Red Sea form a series of high-amplitude highs and lows elongated subparallel to the strike of the rift (Fig. 4), Martinez & Cochran (1988) interpreted them as arising from a series of large rotated fault blocks.

Gaulier *et al.* (1988a) conducted a seismic survey in the Egyptian half of the northern Red sea that included 13 expanding spread profiles (ESPs). One of these was located less than 20 km

from the coast. It showed a 9.1 km-thick crust with the Moho at a depth of 16.7 km. Depth to the Moho was in the range of 13–14.7 km on nine seismic lines located more than 20 km from the coast that gave either a mantle reflection or a phase interpreted as a mantle reflection. On seven of these lines, the Moho was located at 13.0–13.5 km below the sea surface. Two other lines showed a reflection at 10.5 km below the sea surface that could be either the Moho or an intracrustal reflector (Gaulier *et al.* 1988a). The final ESP was located over the axial

Profile A

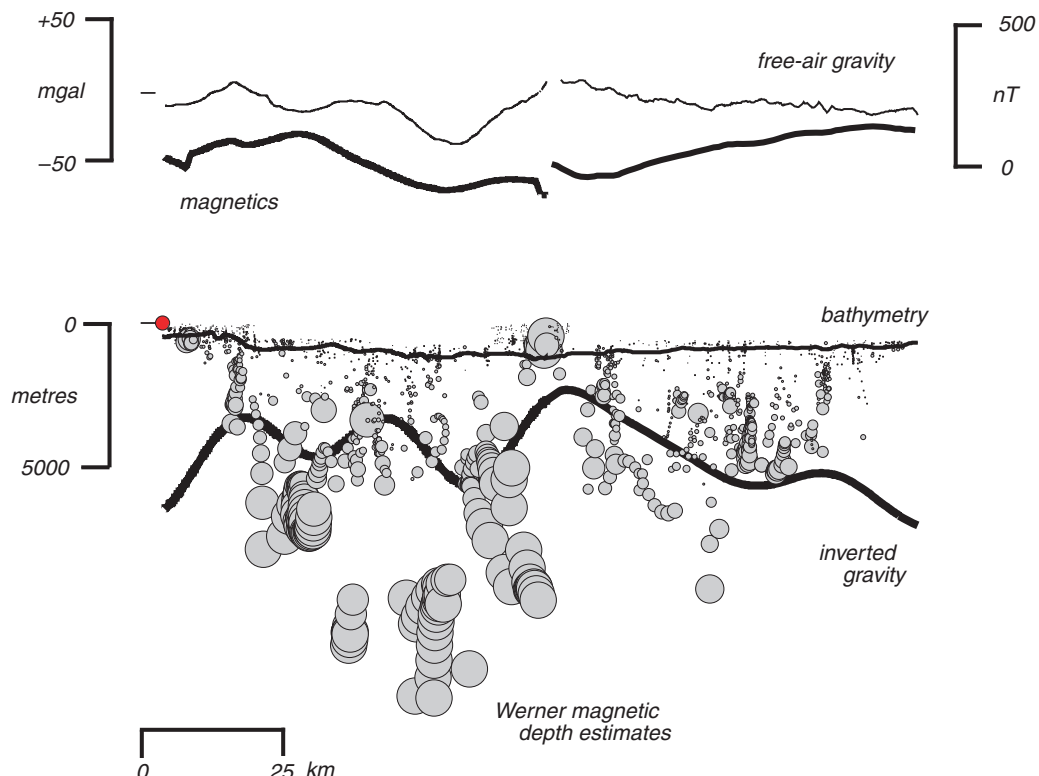


Fig. 3 Single channel reflection seismic (SCS) and projected bathymetry, gravity and magnetic profiles across the northern Red Sea. Parker and Werner deconvolution inversion results show the sediment–basement contact from inversion of gravity anomalies (bold line) and magnetic depth estimates (grey circles), respectively. The Werner circles are the individual depth solutions with circle size being proportional to the magnetic susceptibility. Depth estimates that tend to cluster vertically beneath the true location of the causative body with magnetic basement being interpreted as the top of the vertical ‘streaks’ of the depth solutions. Single channel seismic data (SCS), where available, are also shown. SCS section length is located on each profile. Profiles A–E are located in Figure 2. Profile C is across the Conrad Deep, and shows velocities as a function of depth obtained from the expanding spread seismic experiment of Gaulier *et al.* (1988a, b). Note terraced nature of the bathymetry and the presence of gravity highs on the seaward edge of the terraces. Clustering of Werner solutions on the apexes of the rotated fault blocks gives confidence in the gravity and magnetic inversions.

depression at the location of Conrad Deep, which Cochran *et al.* (1986) argue has been the site of recent large intrusions. This ESP gave an unusual crustal structure with no definable Moho.

The profile shown in Figure 3C is perpendicular to the ESP lines of Gaulier *et al.* (1988a). The location at which the profile crosses each ESP line is noted. A synthetic cross-section from Gaulier *et al.* (1988a) developed from those ESP lines is also shown in Figure 3C. The flat Moho determined from the seismic data is very obvious in the profile. The crustal thickness on the ESPs varied from 5.1 to

8.3 km (Gaulier *et al.* 1988a) with changes in crustal thickness largely corresponding to relief on the top of the crust. The nearly flat Moho requires that the faults bounding these large crustal fault blocks sole out into a horizontal shear zone in the lower crust or at the Moho. The nearly flat Moho also implies that extension has been distributed across the water-covered portion of the rift.

Magnetic anomalies throughout the northern Red Sea north of the Mabahiss Deep pull-apart basin (centred near 25°20'N, 36°10'E, Fig. 2) are all dipolar anomalies (Fig. 5), implying compact,

Profile B

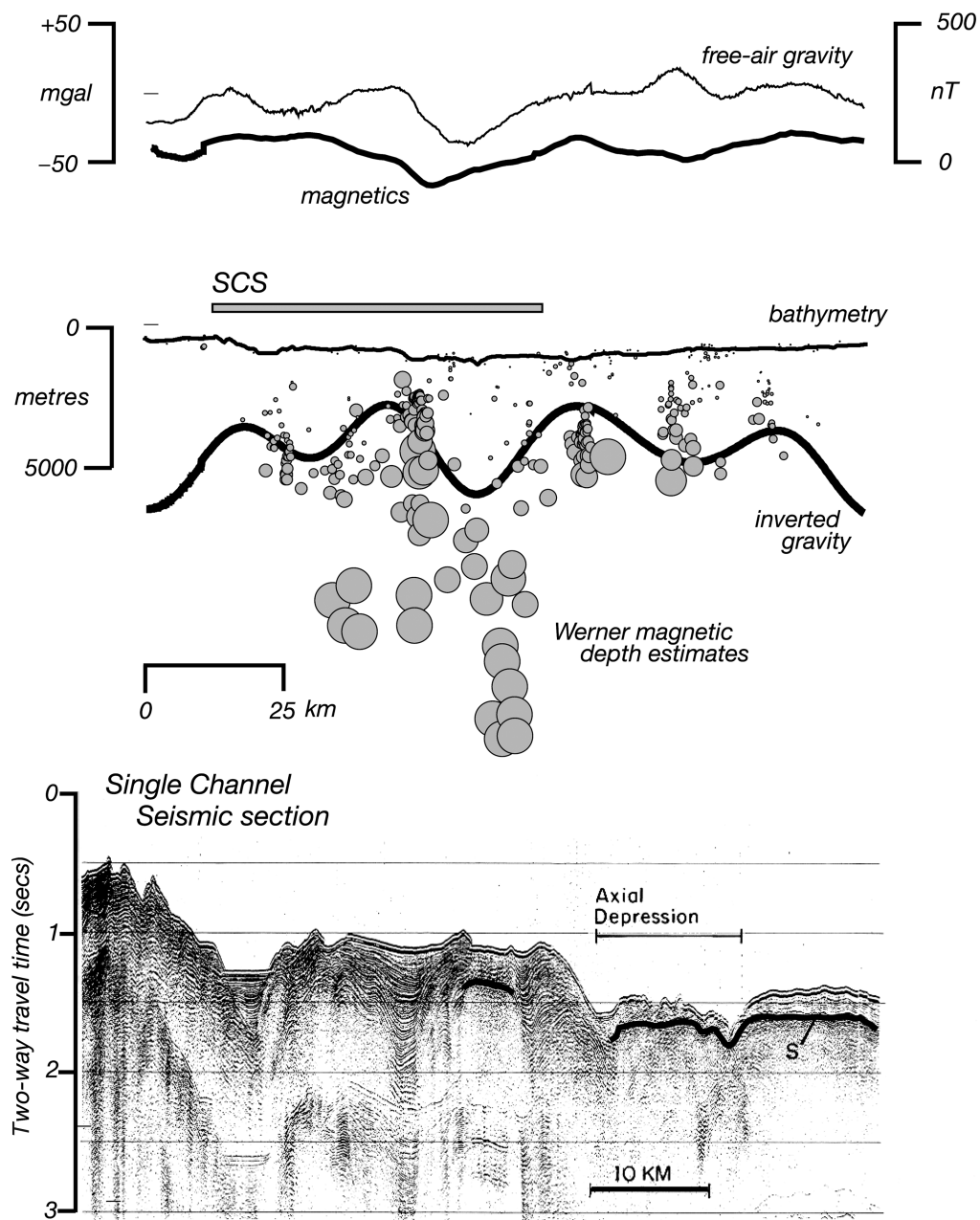


Fig. 3. (Continued)

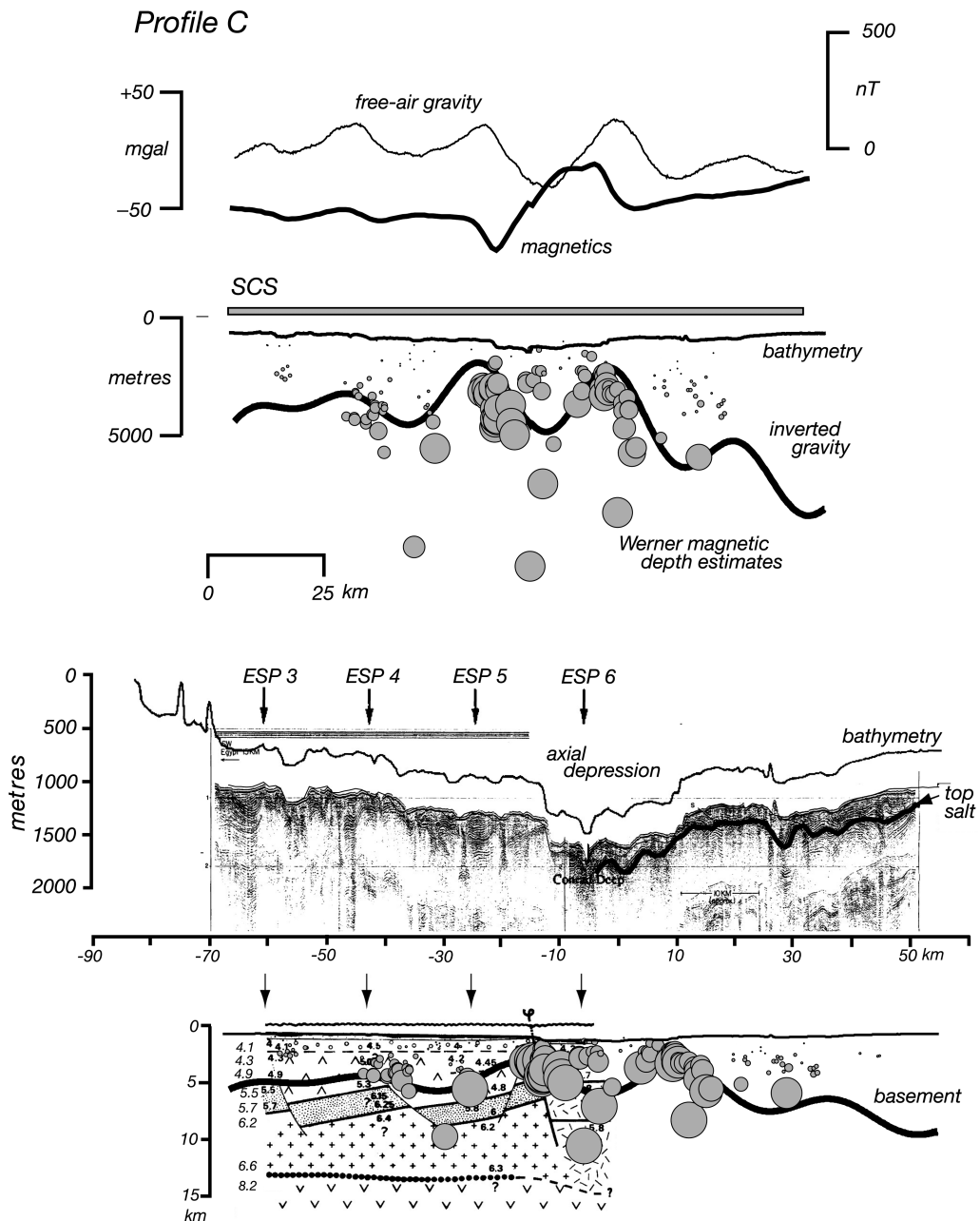


Fig. 3. (Continued)

localized sources (Cochran 2005). These anomalies have been interpreted as arising from individual volcanoes or intrusions (Cochran *et al.* 1986; Guennoc *et al.* 1988; Martinez & Cochran 1988; Cochran 2005). This interpretation has been documented in some cases by observation of a volcanic edifice

associated with the magnetic anomaly (Guennoc *et al.* 1988; Martinez & Cochran 1988; Cochran 2005). The dipolar anomalies in the northern Red Sea all imply normally magnetized sources, suggesting that the volcanoes all formed within the past 780 ka.

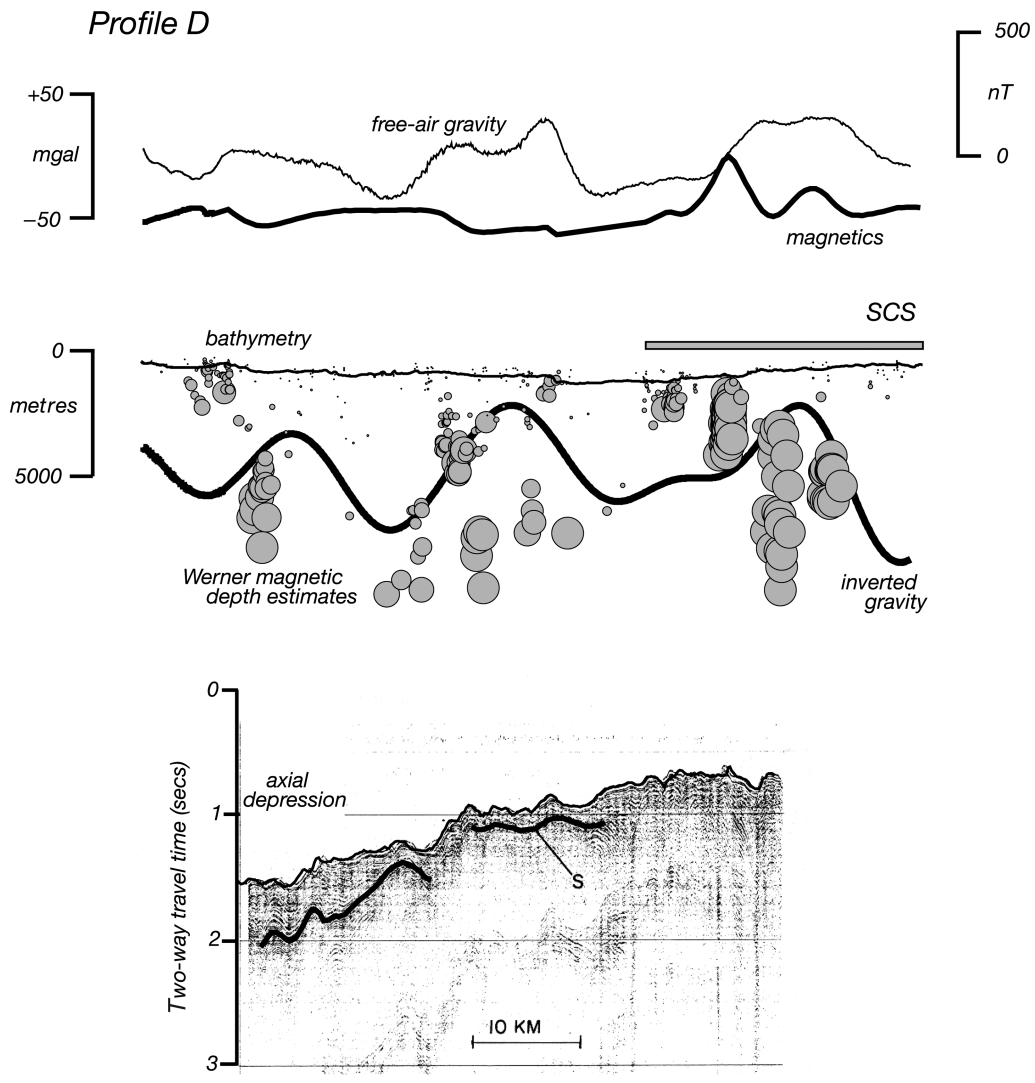


Fig. 3. (Continued)

Volcanoes in the northern Red Sea are systematically found at two locations; at the top of scarps bounding the axial depression and along the edge of terraces in the main trough, particularly where the terraces intersect accommodation zones (Cochran 2005). In both cases it appears that melt ascended along faults (Cochran *et al.* 1986; Cochran 2005). Volcanoes along the edge of the axial depression occur in pairs on opposite sides of the axial depression immediately adjacent to a bathymetric 'deep' within the axial depression with one such pair within each rift segment (Cochran 2005). In one segment, an additional volcano is located on

the floor of the axial depression within Shaban Deep near $26^{\circ}15'N$, $35^{\circ}22'E$ (Pautot *et al.* 1984, 1986) (Fig. 2).

Martinez & Cochran (1988) and Cochran (2005) interpret the development of volcanoes at the axial depression as the first step in the establishment of a magmatic spreading centre within the northern Red Sea. According to their model, lithospheric extension and thinning has become concentrated under the axial depression over the past several million years (Buck *et al.* 1988; Martinez & Cochran 1989). They hypothesize that melt developed under a rift segment is focused along the segment,

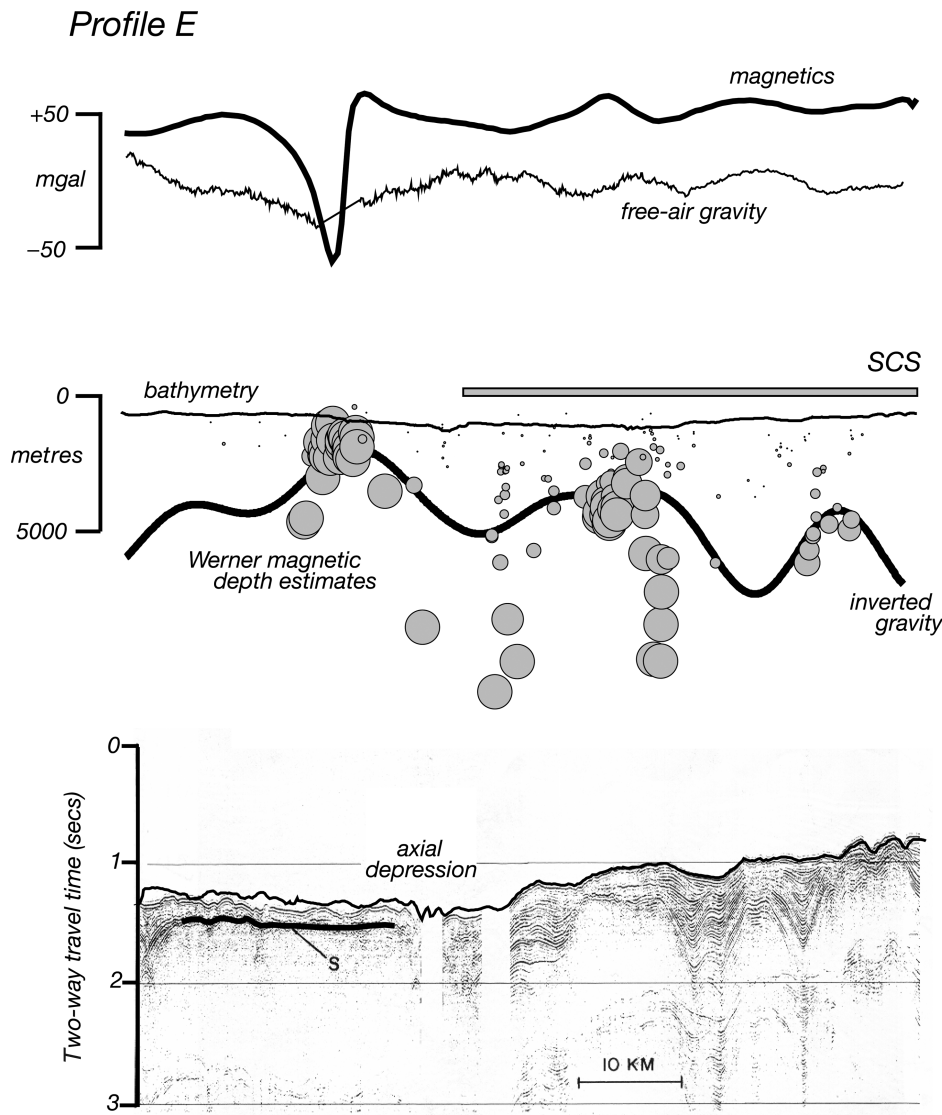


Fig. 3. (Continued)

and then ascends to the surface, originally along faults to form the volcanoes perched on the edge of the axial depression and then directly to form volcanoes in the axial depression, such as observed at Shaban Deep (Pautot *et al.* 1984; Maury *et al.* 1985). These volcanoes develop into isolated cells of sea-floor spreading, as observed in the central Red Sea (Cochran 1983; Pautot 1983; Bonatti 1985; Bicknell *et al.* 1986). These cells are postulated to propagate and grow until they form a continuous axis. The southern, central and northern Red Sea, therefore, represent different stages of

this process of developing an oceanic spreading centre within a continental rift.

If an oceanic axis is developing in the northern Red Sea, as proposed by Martinez & Cochran (1988) and Cochran (2005), the structure of the extended continental crust and the transition to oceanic crust differs significantly from that observed at some other margins including the well-studied margin west of the Iberian Peninsula and the Exmouth Plateau of NW Australia, the Iberian margin being considered the type-example of a non-volcanic rifted margin (e.g. Boillot & Froitzheim

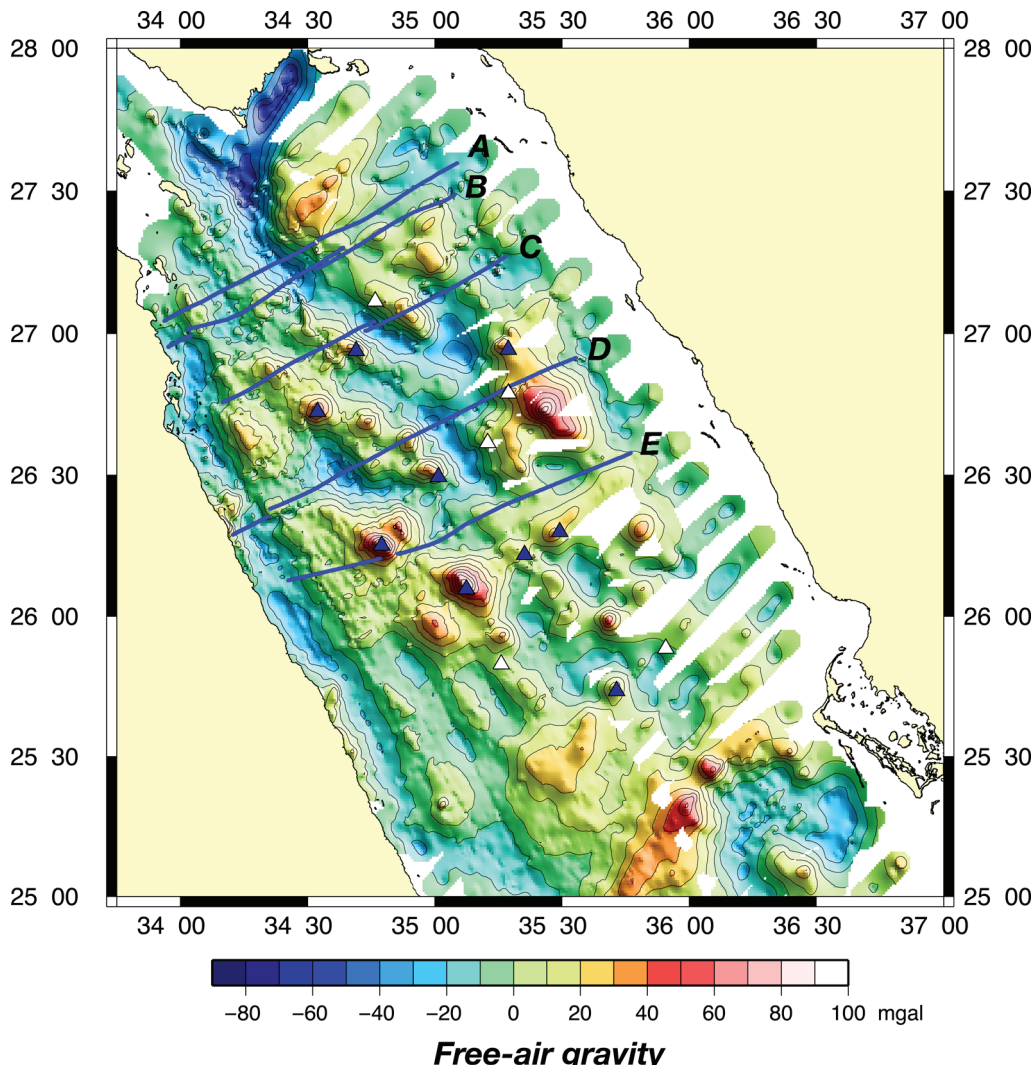


Fig. 4. Northern Red Sea free-air gravity anomaly map contoured at 10 mGal intervals. Data sources for the gravity are discussed by Cochran (2005). Projected shipboard bathymetry, gravity and magnetic data profiles used in the Parker and Werner inversions are shown as blue lines (labelled A–E). Triangles mark location of volcanoes identified from the magnetic anomalies. Triangles are blue when the identification is confirmed by bathymetry and/or gravity data and white when based only on interpretation of the magnetic data. Note the sequence of NNE–SSE linear trending gravity anomalies across the entire region, suggestive of the location of large, rotated fault blocks.

2001; IODP 2001; Whitmarsh *et al.* 2001). In the Red Sea, thinned continental crust with a thickness of at least 5 km extends to the site of volcanic activity at the axial depression (Gaulier *et al.* 1988b). There is no evidence of a zone of exposed mantle rocks, as has been observed at the Iberian margin (e.g. Pickup *et al.* 1996; Chian *et al.* 1999). This difference appears to be reflected in the observation that the distance from basically un rifted

continental crust to the axial depression in the northern Red Sea is about 80 km, much less than the average width of over 200 km for this region at the Iberian margin (e.g. Dean *et al.* 2000). In these respects, the northern Red Sea appears to resemble the Goban Spur margin of the UK, where thin continental crust with a thickness of about 7 km directly abuts oceanic crust (Peddy *et al.* 1989; Horsefield *et al.* 1993) and the width

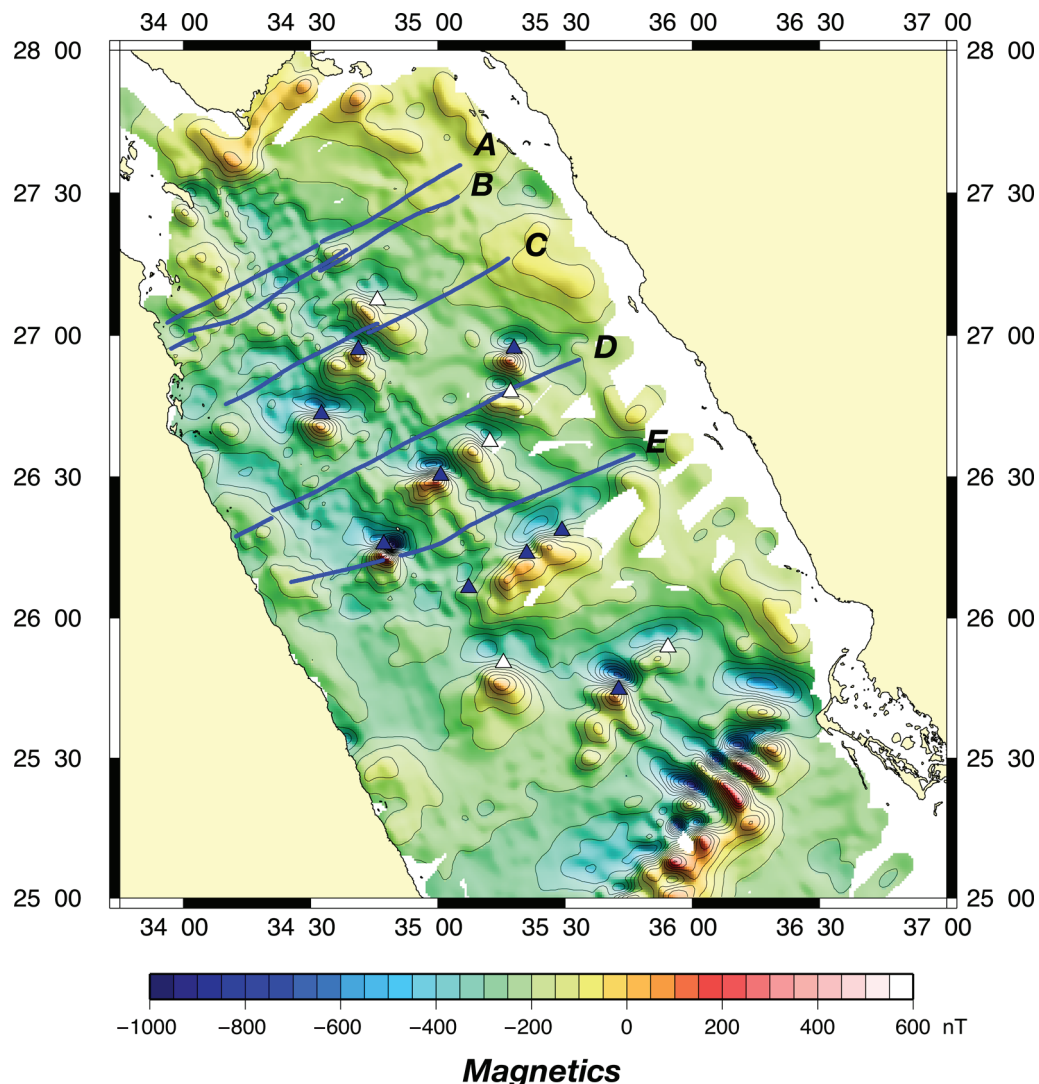


Fig. 5. Total intensity magnetic anomaly map of the northern Red Sea contoured at 50 nT intervals. Data sources for the magnetics are discussed by Cochran (2005). Projected shipboard bathymetry, gravity and magnetic data profiles used in the Parker and Werner inversions are shown as blue lines (labelled A–E). Triangles mark location of volcanoes identified from the magnetic anomalies. Triangles are blue when the identification is confirmed by bathymetry and/or gravity data and white when based only on interpretation of the magnetic data. While large, isolated magnetic anomalies exist in the central region of the northern Red Sea, well developed, linear magnetic anomalies as part of a sea-floor spreading sequence do not exist.

of extended continental crust is also about 80 km (Dean *et al.* 2000).

Discussion

Crustal extension in the northern Red Sea

The model for the transition from rifting to sea-floor spreading in the Red Sea developed by Martinez &

Cochran (1988) and Cochran (2005) assumes that crustal extension in the northern Red Sea during the rifting stage is accomplished mechanically by rotational faulting of crustal blocks accompanied by ductile flow in the lower crust. The upper surface of the crust is thus postulated to consist of a series of large-relief rotated fault blocks. This assumption is based on two observations. First, in the Gulf of Suez, the presence of large faulted

blocks has been confirmed by seismic imaging and well data (e.g. Patton *et al.* 1994; Bosworth 1995; Salah & Al Sharhan 1996; Bosworth & McClay 2001). As the Gulf of Suez was a northern continuation of the Red Sea until the establishment of the Dead Sea transform in the middle Miocene caused extension to be essentially abandoned within the Gulf of Suez, it is assumed that they had a common evolution up to that time.

The second observation is the presence of large-amplitude, elongate gravity highs and lows trending subparallel to the trend of the rift (Martinez & Cochran 1988). Gravity highs are systematically located on the seaward edges of bathymetric terraces (Fig. 3) (Cochran 2005) and are considered to be sourced by basement relief (Martinez & Cochran 1988). We suspect that large fault blocks characterize northern Red Sea extension and will investigate this further by inverting the potential field data across the Red Sea (both gravity and magnetic data). Specifically, we will downward continue the Bouguer gravity anomaly a depth of 5 km, which is the average depth below sea level of the basement (Gaulier *et al.* 1988b), and expand the resulting equivalent mass layer to determine if the required relief is reasonable and compatible with other geological and geophysical constraints. We will also use Werner deconvolution of magnetic data, which will give estimates to the depth of magnetic source. These estimates should help constrain the gravity inversion by identifying areas of steep basement slopes (i.e. the edges of rift blocks). The robustness of the technique is such that no reduction to the magnetic pole is required and the inversion is applicable for either remnant or induced magnetizations.

Gravity inversion. Figure 6 shows a Bouguer gravity anomaly map of the northern Red Sea calculated using a density contrast of 1370 kg m^{-3} . This density contrast was chosen to eliminate the gravity effect of bathymetric relief, which arises from the density contrast between sea water and sediments (assumed to have an average density of 2400 kg m^{-3} (Martinez & Cochran 1988). We calculated the gravity effect of the sediment–water interface using four terms in the Parker (1973) fast Fourier transform technique. The resulting grid was sampled at the locations of the free-air gravity measurements, these values subtracted point-by-point from the free-air anomalies, and the resulting point Bouguer anomalies gridded in the same manner as was done with the point free-water gravity anomaly values. The Bouguer anomalies shown in Figure 6 have also had a regional planar trend removed. The Bouguer anomaly has greatly reduced the amplitude of the large negative gravity anomaly over the axial depression (Figs 4 & 6), but

the lineated gravity highs and lows observed in the free-air gravity anomalies are still present as the dominant feature in the Bouguer anomaly map.

As the Moho in the northern Red Sea appears to be basically flat (Gaulier *et al.* 1988b) (Fig. 3C), we will assume that the Bouguer gravity anomalies result from relief on the sediment–basement interface and calculate the amount of relief on that surface required to produce them. We downward continued the Bouguer anomalies from the sea surface to a depth of 5 km, the average depth to top of the crust estimated from the seismic lines of Gaulier *et al.* (1988b). Since downward continuation is inherently unstable at short wavelengths, we first applied a low-pass filter to the gravity data that removed all wavelengths less than 20 km and passed wavelengths greater than 30 km. The downward continued gravity anomalies were converted to an equivalent mass layer and relief on that surface determined assuming a density contrast of 400 kg m^{-3} across the sediment–crust interface.

We then calculated the gravity effect of the resulting basement surface using four terms in the Parker (1973) technique, sampled the resulting grid at the locations of gravity measurements, subtracted these values from the Bouguer anomalies and gridded the resulting residual anomalies in the same manner as had been done for the Bouguer anomalies. The residual anomalies were filtered, downward continued and converted to basement relief in the manner described above. This residual basement relief was added to that determined in the first step to produce the calculated depth to the top of the crust shown in Figure 7. As would be expected, the calculated relief resembles a filtered version of the gravity anomalies with a series of elongated highs and lows. Because of the filtering necessary to stabilize the inversion, the result has a rounded appearance rather than the asymmetric rectilinear shape characteristic of fault blocks (i.e. the apexes of the blocks have been smoothed). The gravity effect of the calculated basement relief is shown in Figure 8. The filtered residuals between the Bouguer gravity anomalies (Fig. 7) and the calculated gravity (Fig. 8) are consistently less than about 2–3 mGal except in the vicinity of Mabahiss Deep (Fig. 9). The low residual values in Figure 9 indicate that the predicted basement relief explains basically all of the gravity ‘energy’.

The inferred top of crust is generally at a depth of 2–8 km below sea level with the relief of about 2–6 km between adjacent highs and lows. The computed basement surface nearly reaches the sea surface near $26^{\circ}16'N$, $34^{\circ}47'E$ where a bathymetric peak interpreted as a volcano (Martinez & Cochran 1988) comes to within 300 m of the surface on a bathymetric profile. The only location where the

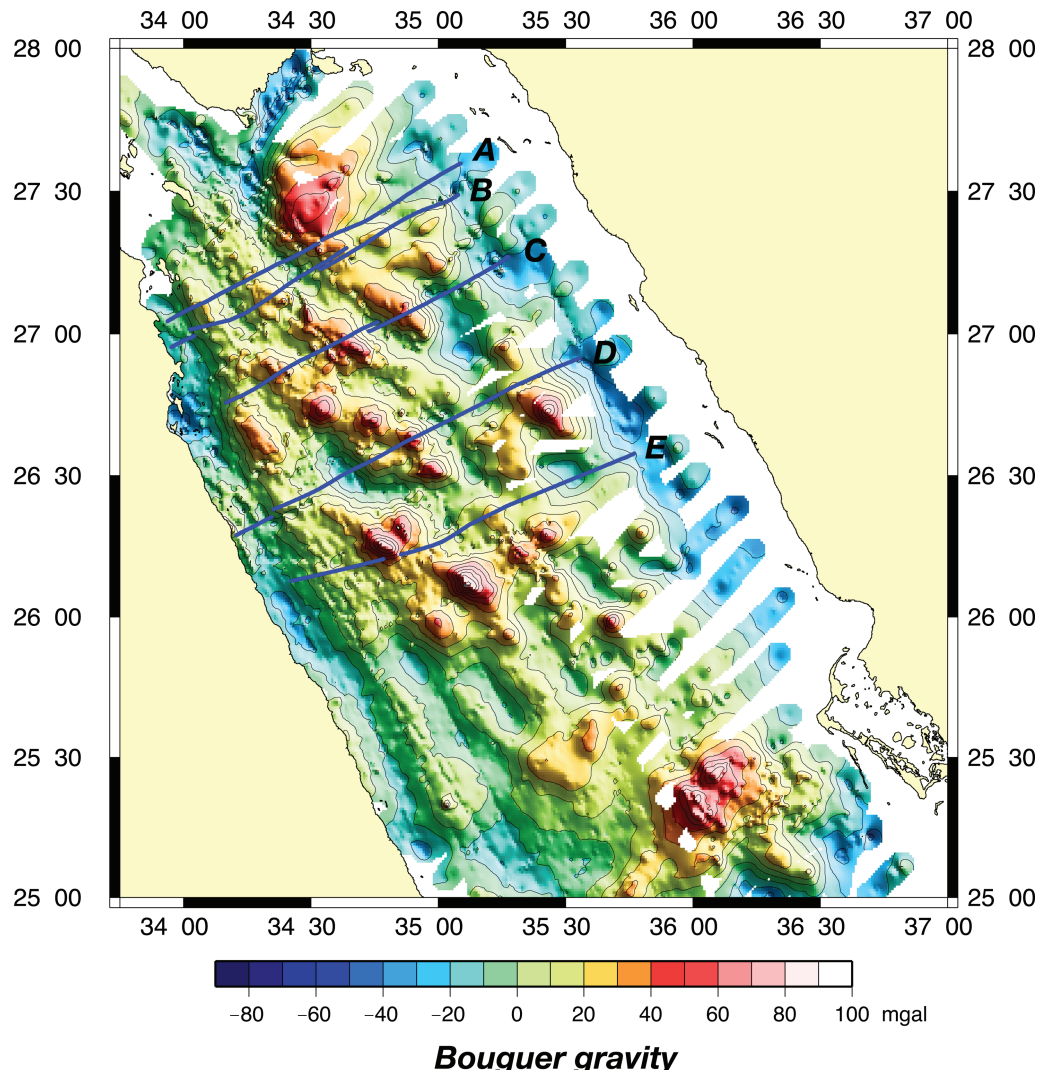


Fig. 6. Northern Red Sea Bouguer gravity anomaly map contoured at 10 mGal intervals and assuming a Bouguer reduction density of 1370 kg m^{-3} (topographic density of 2400 kg m^{-3} and water density of 1030 kg m^{-3}). Projected shipboard bathymetry, gravity and magnetic data profiles used in the Parker and Werner inversions are shown as blue lines (labelled A–E).

computed top of the crust comes above the sea surface is near $26^{\circ}44'\text{N}$, $35^{\circ}26'\text{E}$, where it extends a few hundred metres above sea level. This is the location of a large gravity high (Figs 4 & 6) located in an area of sparse data (Cochran 2005), so it is unclear how well constrained this anomaly is by the data. Although our 5 km average basement depth should perhaps have been slightly deeper, the gravity inversion produces basement relief that is reasonable and consistent with available seismic results supporting the conclusion of Martinez &

Cochran (1988) that the northern Red sea is underlain by a series of large crustal fault blocks.

The Werner deconvolution method. Magnetic data are often used to estimate the depth of magnetic basement in sedimentary basins and passive continental margins (e.g. Grant & West 1965; Klitgord & Behrendt 1979). This is possible because, in general, the sediments within a basin have relatively weak magnetic susceptibilities compared with those of crystalline–volcanic basement at the base of the

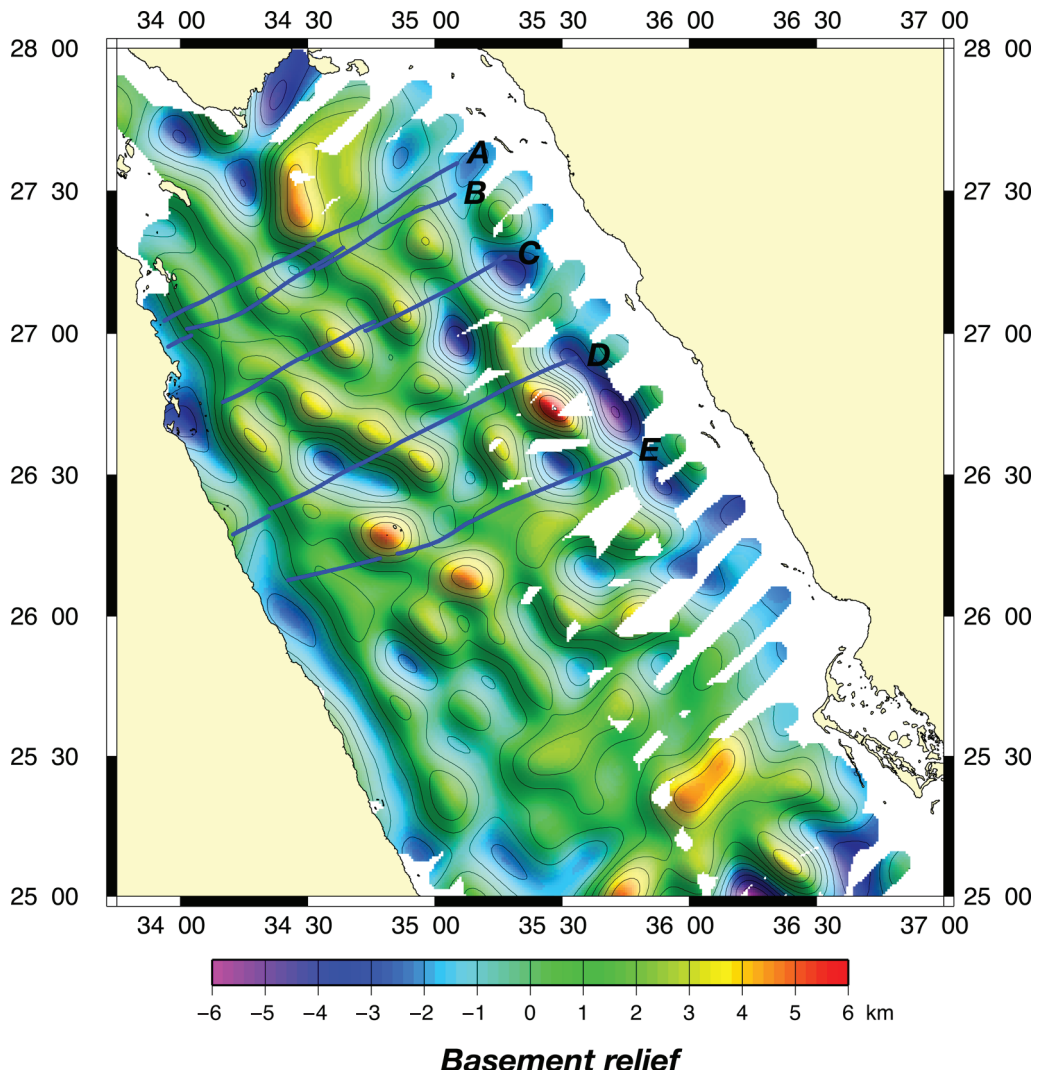


Fig. 7. Predicted, relative sediment–basement contact obtained by inverting the Bouguer gravity of the northern Red Sea region contoured at 1 km intervals. Maximum range in basement relief is 2–8 km below sea level (eastern edge of region between Profiles D and E) with an average relief of about 2–6 km between adjacent highs and lows. A constant sediment–basement density contrast of 400 kg m^{-3} was assumed. Projected shipboard bathymetry, gravity and magnetic data profiles used in the Parker and Werner inversions are shown as blue lines (labelled A–E).

sediment column. Werner (1953) recognized that the usual approach to magnetic interpretation, that of analysing discrete anomalies using such parameters as maxima, minima, inflection points or other intrinsic properties of the observed magnetic anomaly profile, was complicated because of the interference of adjacent anomalies and the effect of noise (e.g. diurnal variations, non-two-dimensionality and induced v. remnant magnetism). For this reason, our Werner deconvolution algorithm uses simple

models for the source and a quadratic form for the source/noise interference to determine the magnetization properties of the causative bodies. The basic assumption of the approach is that all magnetic anomalies are the result of either a sequence of dykes or an interface between juxtaposed half-spaces of different magnetic susceptibility. In particular, the strike length and depth of the causative body are assumed to be infinite while the width of the body is assumed to be either: (1) finite, representing a

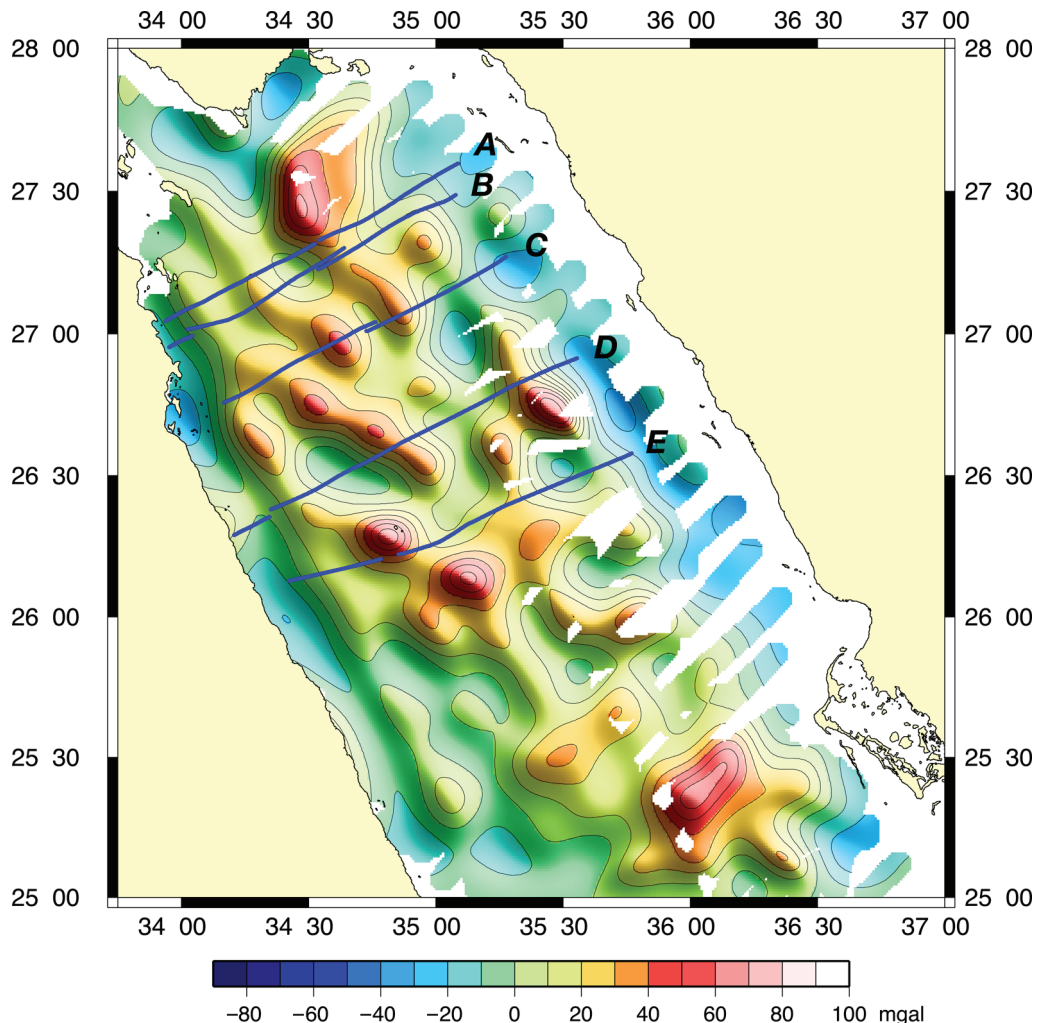


Fig. 8. Calculated gravity effect of the predicted basement relief shown in Figure 7. This is used to ascertain how much energy is being ‘captured’ by the predicted relief. A constant sediment–basement density contrast of 400 kg m^{-3} was assumed. Projected shipboard bathymetry, gravity and magnetic data profiles used in the Parker and Werner inversions are shown as blue lines (labelled A–E).

dyke; or (2) approaching zero such that it represents an interface between two regions of differing magnetic susceptibility. The robustness of the technique is such that no reduction to the pole is required and works effectively with both induced and remnant magnetizations.

We have used five dip lines for gravity and magnetic inversion analysis (Fig. 3). To interpret Werner estimates requires knowledge of the role of the data window. For a given pass and data spacing, 11 points are used to estimate a depth, magnetization intensity and magnetization dip. As the window is made wider, deeper magnetic

sources can be potentially recognized. Depth estimates for a ‘true’ shallow source will usually be biased to deeper depths for increasing window lengths. If the deconvolution is successful in defining a ‘real’ magnetic body, then depth estimates should define either the edges of the causative body or the depth range of an interface or the upper boundary of a dyke.

Shown in Figure 3A–E are the results of the Werner depth estimates to magnetic source compared with the inversion of the free-air gravity anomalies described above. In general, it is not possible to see any structure below the evaporites

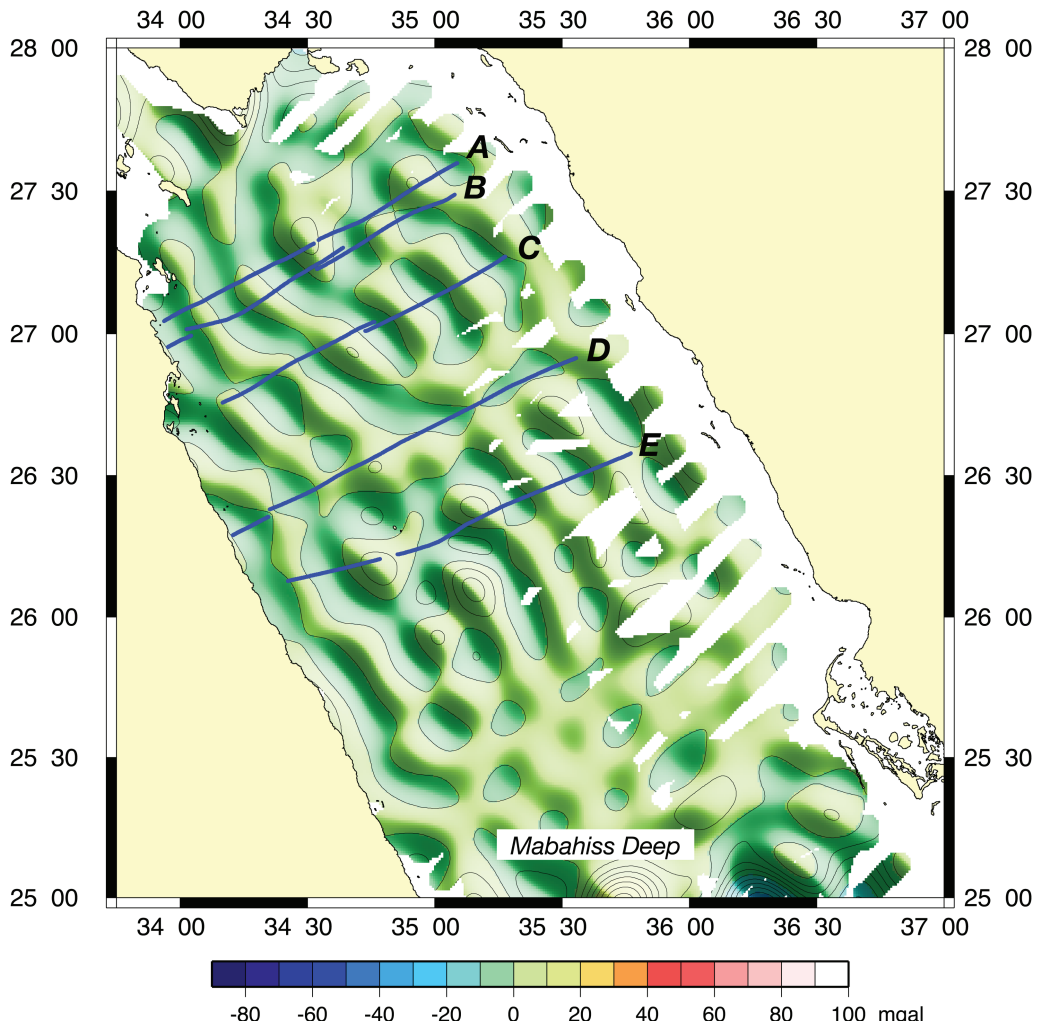


Fig. 9. Filtered residual gravity anomaly obtained by subtracting the gravity effect of the predicted basement relief from the Bouguer gravity anomaly. Contour interval is 10 mGal. Projected shipboard bathymetry, gravity and magnetic data profiles used in the Parker and Werner inversions are shown as blue lines (labelled A–E).

as imaged by the single-channel seismic data. Magnetic estimates are of two types: (1) volcanic intrusions (e.g. Fig. 3D); or (2) the apex of tilted fault blocks, consistent with rift structure across the northern Red Sea based on crustal refraction velocities determined from expanding spread seismic profiles (Fig. 3C) (Gaulier *et al.* 1988a, b). There is excellent agreement between the smoothed, sediment–basement relief and geometry, and the depth to the fault block apex using the magnetic data. We conclude from the gravity and magnetic inversion that the northern Red Sea consists primarily of extended continental crust characterized by a series of large rotated crustal fault blocks.

When will sea-floor spreading develop in the northern Red Sea, if ever?

Martinez & Cochran (1988) and Cochran (2005) have proposed a model for the development of an oceanic spreading centre within a continental rift based on observations in the northern Red Sea. They suggest that rift development occurs through rotation of large crustal fault blocks along listric faults that sole out into a zone of plastic creep, resulting in a flat Moho and high upper crustal relief, as observed in the northern Red Sea (Fig. 3). This initial, broadly distributed extension eventually becomes centred at the rift axis leading

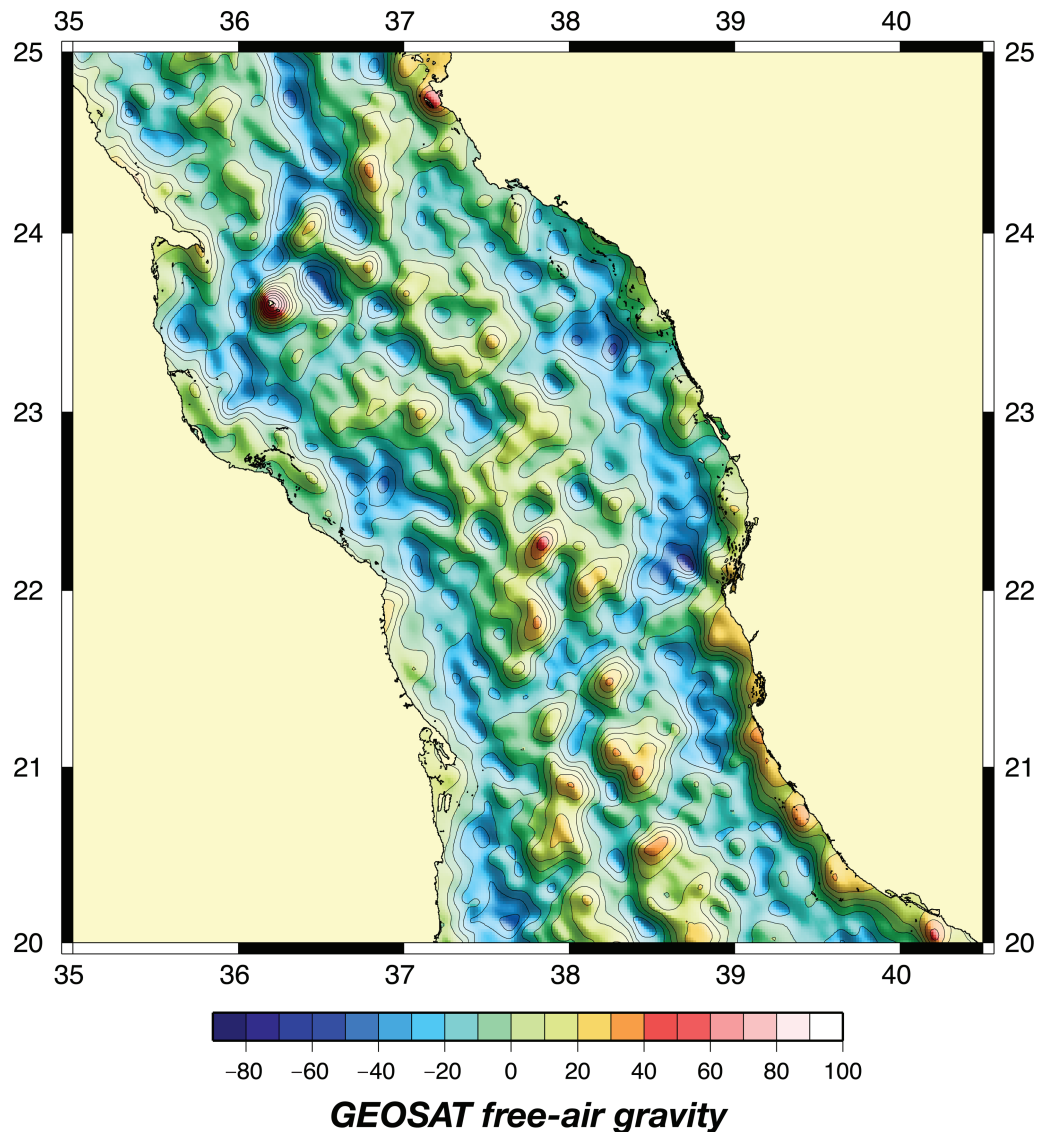


Fig. 10. Satellite free-air gravity map of the central Red Sea using the 1×1 min world grid from Smith & Sandwell (1997; version 15.1). Contour interval is 10 mGal.

to rapid lithospheric thinning and melt generation (Buck *et al.* 1988). Melt formed within individual rift segments is focused to a location within the segment to form small axial volcanoes at the axis (Cochran 2005). With continued extension and magmatism, these volcanoes become cells of sea-floor spreading as observed in the central Red Sea (Degens & Ross 1969; Backer *et al.* 1975; Bonatti 1985; Bicknell *et al.* 1986). The deeps then propagate along axis and coalesce to form a continuous axis, as is observed in the southern Red Sea

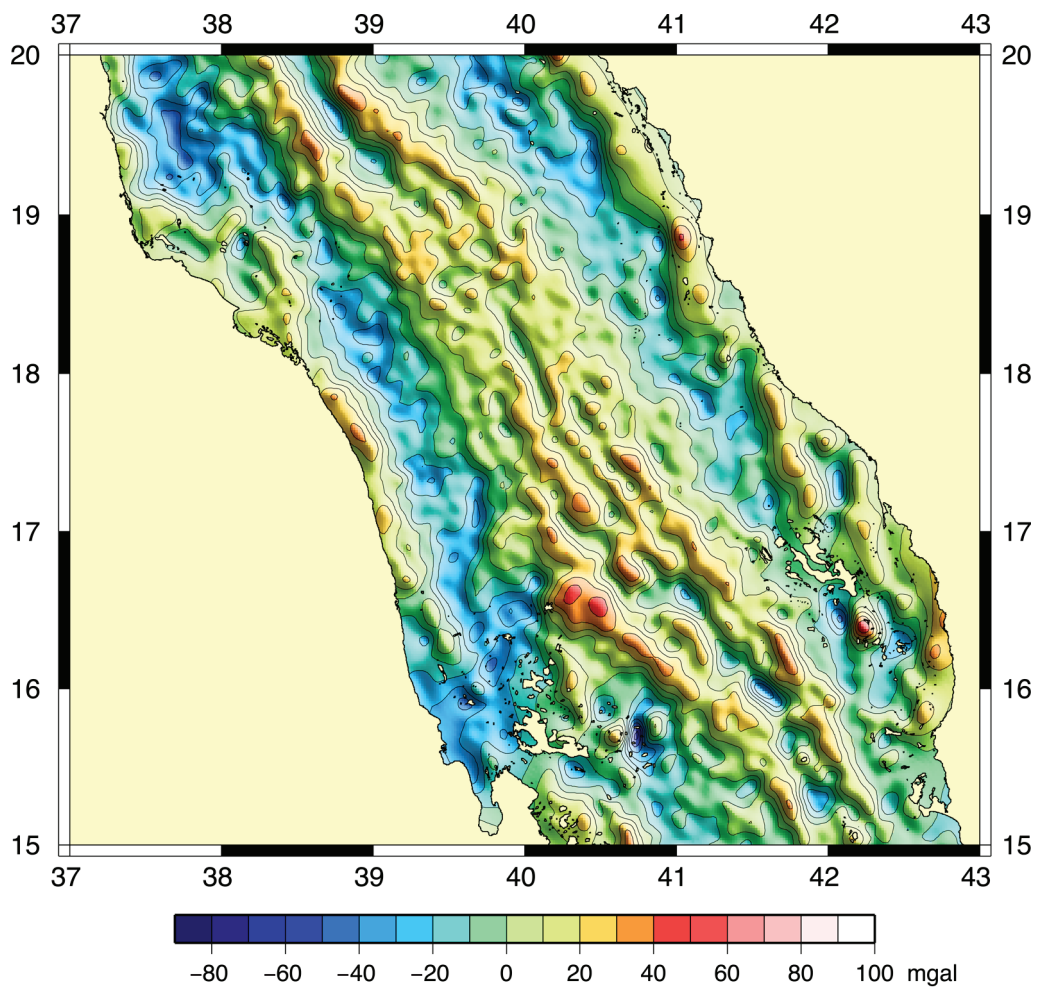
(Roeser 1975; Cochran 1983). According to this model, the northern Red Sea is on the verge of replacing horizontal translation with focused mantle upwelling and organized sea-floor spreading.

A corollary of this hypothesis is that the tectonic processes that have shaped the northern Red Sea have been active throughout the entire Red Sea and that the tectonic framework deduced in the north continues to the south. Thus, it is expected that the large rotated fault blocks found in the Gulf of Suez and the main trough of the northern

Red Sea are also present in the main trough of the central and southern Red Sea. There is presently insufficient data from the central and southern Red Sea to construct free-air or Bouguer gravity maps based on surface ship data. However, free-air anomaly maps derived from satellite altimetry data (Figs 10 & 11) do not show the prominent linear rift-parallel gravity highs and lows that characterize the northern Red Sea. This does not appear to be due to differing resolution in the surface and altimetry data because the linear gravity anomalies characteristic of the northern Red Sea are evident in satellite altimetry data (Cochran 2005). In addition, a reflector interpreted

as main trough basement by Izzeldin (1987) on a 48-channel seismic reflection line across the Red Sea between 20°N and 21°N does not show the presence of high-relief fault blocks.

In marked contrast to the structure observed in the northern Red Sea, Karner *et al.* (2003) and Karner (2005) have shown that the West African and Brazilian passive continental margins are characterized by the stacking of regional synrift sag basins, the amplitude and distribution of which are inconsistent with the minor amounts of brittle deformation mapped from seismic sections. The sag basins exhibit none of the diagnostic features expected of synrift extensional systems



GEOSAT free-air gravity

Fig. 11. Satellite free-air gravity map of the southern Red Sea using the 1 × 1 min world grid from Smith & Sandwell (1997; version 15.1). Contour interval is 10 mGal.

(e.g. normal faults that control accommodation, rotation of crustal blocks, prominent rift onset unconformities, synrift sediment wedges). Large post-rift subsidence in regions characterized by relatively minor synrift faulting is most easily explained by depth-dependent extension that is partitioned vertically across a zone of decoupling separating a relatively non-deforming upper crust (upper plate) from a ductile-deforming lower crust and lithospheric mantle (lower plate; Karner *et al.* 2003). A fundamental implication of this model is that rifts characterized by large offset fault systems, that is faults that generate synrift accommodation such as in the Basin and Range province, East African rift system, North Sea Basins, Rhinegraben and Newark Basin, will not proceed to breakup. Thus, according to this model, because of the existence of large fault blocks in the northern Red Sea, it should not proceed to sea-floor spreading.

A possible reason for different responses to lithospheric extension in the northern and southern Red Sea is alteration and weakening of the lithosphere as a result of the impact of the Afar plume head at about 30 Ma. Although the massive burst of volcanism that accompanied impingement of the plume head on the lithosphere is concentrated in Ethiopia and southern Yemen, significant coeval volcanism is reported as far north as 18°N in the Red Sea hills of Eritrea and Sudan (Drury *et al.* 1994; Kenea *et al.* 2001). Drury *et al.* (1994) describe basalt flows reaching a preserved thickness of 600 m that were erupted 32.9 and 28 Ma in northern Eritrea. Kenea *et al.* (2001) describe exposures of identically aged basalt flows with an aggregate thickness of at least a few hundred metres from more than 200 km further north in Sudan. They argue that flood basalts were erupted across an area approximately 1000 km in diameter between about 31 and 28 Ma, prior to onset of any known extension or plateau uplift. The ellipse drawn by Kenea *et al.* (2001) to illustrate the extent of the Afar flood basalt province extends to almost 20° in the Red Sea and corresponds to the portion of the Red Sea with a well-developed mid-ocean ridge (Roeser 1975; Cochran 1983).

Further evidence that the lithosphere in the southern Red Sea may have been weakened and made more susceptible to stretching and melting is given by along-strike variations in the character of the 24–21 Ma dyke event that occurred along the entire length of the rift in Arabia (Blank 1977; Feraudet *et al.* 1991) and into the Sinai (Bartov *et al.* 1980), which marks the beginning of extension and synrift sediment deposition (Bosworth *et al.* 2005). North of Jeddah, the dykes crop out discontinuously and their presence and continuity along strike is determined primarily from linear,

high-amplitude magnetic anomalies (Blank 1977; Eyal *et al.* 1981). South of Jeddah, the dyke swarm becomes much more intense (Coleman *et al.* 1983; Coleman & McGuire 1988), crops out over wide areas, and is accompanied by large, intrusive igneous complexes in at least two locations, Al Lith near 21°N (Pallister 1987) and Tihama Asir near 17°N (Coleman *et al.* 1979, 1983). The two igneous complexes give an $^{40}\text{Ar}/^{39}\text{Ar}$ age range that coincides with those of the dykes (Feraud *et al.* 1991; Sebai *et al.* 1991).

Courtillot *et al.* (1999) have argued that there is a causal link between the impingement of plume heads on the lithosphere and continental breakup to form new ocean basins. In the case of the Red Sea, it is possible that Afar plume head affected the lithosphere north to about 21–22°N, so that when extension began, 5–7 Ma later, the region of weakened lithosphere responded in a different manner than did the unmodified lithosphere of the northern Red Sea.

Conclusions

The northern Red Sea has been undergoing continental rifting and extension since 24–21 Ma. The crust within the rift is now 5 to 8 km thick with a nearly flat Moho (Gaulier *et al.* 1988b). From our gravity and magnetic analysis, sediment thicknesses range from 2–8 km with an average of approximately 5 km. Martinez & Cochran (1988) have hypothesized that large-amplitude, linear gravity highs and lows observed in the main trough of the northern Red Sea result from relief on a series of large rotated crustal fault blocks making up the upper crust. We have also shown that this hypothesis is consistent with the inversion of the gravity and magnetic data.

There is a transition in the northern Red Sea from continental rifting in the north to sea-floor spreading in the south. As the opening rate is twice as great in the south, this is widely interpreted to reflect the northward propagation of organized sea-floor spreading (e.g. Courtillot 1980, 1982; Cochran 1983, 2005; Bonatti 1985). However, gravity anomalies derived from satellite altimetry data do not show large, linear, rift-parallel gravity anomalies in the main trough of the central and southern Red Sea where oceanic spreading centres have developed. This raises the possibility that continental extension in the northern and southern portions of the Red Sea has been accommodated in different manners, with large rotated fault blocks formed in the northern Red Sea and regional synrift sag basins developed in the south. This difference in the crustal architecture, combined with observations of the structure of continental

margins and failed continental rifts in other parts of the world (e.g. Karner *et al.* 2003; Karner 2005), allows speculation that depth-dependent extension leading to development of large sag basins is necessary for continental rifting to proceed to continental lithosphere breaching and the development of an oceanic spreading centre. If this hypothesis is correct, then it is possible that an oceanic spreading centre will not develop in the northern Red Sea. A possible reason for the difference in the response of the lithosphere to extension in the northern and southern Red Sea is the thermal and rheological weakening and alteration of the lithosphere resulting from the impact of the Afar plume head.

This work was supported by National Science Foundation grants OCE-9819563, OCE-0548812 (J.R. Cochran) and OCE-0425411 (G.D. Karner). The GMT software package (Wessel & Smith 1998) was used extensively in the preparation of figures. LDEO publication 7010.

References

- ABBATE, E., BELESTIERI, M. L. & BIGAZZI, G. 2002. Morphostructural development of the Eritrean rift flank (southern Red Sea) inferred from apatite fission track analysis. *Journal of Geophysical Research*, **107**, 2319, doi:10.1029/2001JB001009.
- BACKER, H., LANGE, K. & RICHTER, H. 1975. Morphology of the Red Sea Central Graben between Subair Islands and Abul Kizaan. *Geologische Jahrbuch*, **D13**, 79–123.
- BADAWY, A. 2005. Seismicity of Egypt. *Seismology Research Letters*, **76**, 149–160.
- BAKER, J., SNEE, L. & MENZIES, M. A. 1996. A brief Oligocene period of flood basalt volcanism in Yemen: implications for the duration and rate of continental flood volcanism at the Afro-Arabian triple junction. *Earth and Planetary Science Letters*, **138**, 39–55.
- BARTOV, Y., STEINITZ, G., EYAL, M. & EYAL, Y. 1980. Sinistral movement along the Gulf of Aqaba—its age and relation to opening of the Red Sea. *Nature*, **285**, 220–221.
- BAYOUMI, A. I. & LOFTY, H. I. 1989. Modes of structural evolution of Abu Gharadig Basin, Western Desert of Egypt as deduced from seismic data. *Journal of African Earth Science*, **9**, 271–187, 1989.
- BICKNELL, J. D., MACDONALD, K. C., MILLER, S. P., LONSDALE, P. F. & BECKER, K. 1986. Tectonics of the Nereus Deep, Red Sea: A deep tow investigation of a site of initial rifting. *Marine Geophysical Researches*, **8**, 131–148.
- BLANK, H. R. 1977. Aeromagnetic and geologic study of Tertiary dikes and related structures on the Arabian margin of the Red Sea. In: *Red Sea Research 1970–1975*. Saudi Arabia Directorate General of Mineral Resources Bulletin, **22**, pp. G1–G27.
- BODHANNON, R. G., NAESER, C. W., SCHMIDT, D. L. & ZIMMERMAN, R. A. 1989. Timing of uplift, volcanism, and rifting peripheral to the Red Sea: A case for passive rifting. *Journal of Geophysical Research*, **94**, 1683–1701.
- BOILLOT, G. & FROITZHEIM, N. 2001. Non-volcanic rifted margins, continental breakup and the onset of sea-floor spreading: some outstanding problems. In: WILSON, R. C. L., WHITMARSH, R. B., TAYLOR, B. & FROITZHEIM, N. (eds) *Non-volcanic Rifting of Continental Margins: A Comparison of Evidence From Land and Sea*. Geological Society, London, Special Publications, **187**, 9–30.
- BONATTI, E. 1985. Punctiform initiation of seafloor spreading in the Red Sea during transition from a continental to an oceanic rift. *Nature*, **316**, 33–37.
- BOSWORTH, W. 1992. Mesozoic and early Tertiary rift tectonics in East Africa. *Tectonophysics*, **209**, 115–137.
- BOSWORTH, W. 1995. A high-strain rift model for the Gulf of Suez (Egypt). In: LAMBIASE, J. J. (ed.) *Hydrocarbon Habitat in Rift Basins*. Geological Society, London, 75–102.
- BOSWORTH, W. & MCCLAY, K. 2001. Structural and stratigraphic evolution of the Gulf of Suez Rift, Egypt: a synthesis. In: ZIEGLER, P. A., CAVAZZA, W., ROBERTSON, A. H. F. & CRASQUIN-SOLEAU, S. (eds) *Peri-Tethys Memoir 6: Peri-Thethyan Rift/Wrench Basins and Passive Margins*. Muséum national d'Histoire naturelle, Paris, 567–606.
- BOSWORTH, W., CREVELLO, P., WINN, R. D. & STEINMETZ, J. 1998. Structure, sedimentation, and basin dynamics during rifting of the Gulf of Suez and northwestern Red Sea. In: PURSER, B. H. & BOSENCE, D. W. J. (eds) *Sedimentation and Tectonics in Rift Basins: Red Sea–Gulf of Aden*. Chapman & Hall, London, 77–96.
- BOSWORTH, W., GUIRAUD, R. & KESSLER, L. G. 1999. Late Cretaceous (ca. 84 Ma) compressive deformation of the stable platform of northeast Africa (Egypt): Far-field stress effects of the ‘Santonian event’ and origin of the Syrian arc deformation belt. *Geology*, **27**, 633–636.
- BOSWORTH, W., HUCHON, P. & MCCLAY, K. 2005. The Red Sea and Gulf of Aden Basins. *Journal of African Earth Sciences*, **43**, 354–378.
- BOTT, W. F., SMITH, B. A., OAKES, G., SIKANDER, A. H. & IBRAHIM, A. I. 1992. Tectonic framework and regional hydrocarbon prospectivity of the Gulf of Aden. *Journal of Petroleum Geology*, **15**, 211–244.
- BOULOS, F. K. 1990. Some aspects of the geophysical regime of Egypt in relation to ground water and micro-earthquakes. In: SAID, R. (ed.) *The Geology of Egypt*. A.A. Balkema, Rotterdam, 51–59.
- BRANNAN, J., GERDES, K. D. & NEWTH, I. R. 1997. Tectono-stratigraphic development of the Qamar basin, Eastern Yemen. *Marine and Petroleum Geology*, **14**, 701–730.
- BUCK, W. R., MARTINEZ, F., STECKLER, M. S. & COCHRAN, J. R. 1988. Thermal consequences of lithospheric extension: Pure and simple. *Tectonics*, **7**, 213–234.
- CAMP, V. E. 1984. Island arcs and their role in the evolution of the western Arabian Shield. *Geological Society of America Bulletin*, **95**, 913–921.

- CHIAN, D., LOUDEN, K. E., MINSHULL, T. A. & WHITMARSH, R. B. 1999. Deep structure of the ocean-continent transition in the southern Iberia Abyssal plain from seismic refraction profiles: Ocean Drilling Program (Legs 149 and 173) transect. *Journal of Geophysical Research*, **104**, 7443–7462.
- CHU, D. & GORDON, R. G. 1998. Current plate motions across the Red Sea. *Geophysical Journal International*, **135**, 313–328.
- COCHRAN, J. R. 1983. A model for the development of the Red Sea. *AAPG Bulletin*, **67**, 41–69.
- COCHRAN, J. R. 2005. Northern Red Sea: Nucleation of an oceanic spreading center within a continental rift. *Geochemistry, Geophysics, Geosystems*, **6**, Q03006, doi:10.1029/2004GC000826.
- COCHRAN, J. R., MARTINEZ, F., STECKLER, M. S. & HOBART, M. A. 1986. Conrad Deep: A new Northern Red Sea Deep. Origin and implications for continental rifting. *Earth and Planetary Science Letters*, **78**, 18–32.
- COLEMAN, R. G. 1984. The Red Sea: a small ocean basin formed by continental extension and seafloor spreading. In: Proceedings of the 27th International Geological Congress—Invited Papers. E. J. Brill USA, Boston, MA, 93–121.
- COLEMAN, R. G. & MCGUIRE, A. V. 1988. Magma systems related to the Red Sea system. *Tectonophysics*, **150**, 77–100.
- COLEMAN, R. G., HADLEY, D. G., FLECK, R. G., HEDGE, C. T. & DONATO, M. M. 1979. The Miocene Tihama Asir Ophiolite and its bearing on the Opening of the Red Sea. In: AL-SHANTI, A. M. S. (ed.) *Evolution and Mineralization of the Arabian–Nubian Shield*. Pergamon, Oxford, 173–186.
- COLEMAN, R. G., GREGORY, R. T. & BROWN, G. F. 1983. Cenozoic Volcanic Rocks of Saudi Arabia. US Geological Survey Open File Report, **82**, 83–788.
- COULIE, E., QUIDELLEUR, X., GILLOT, P. Y., COURTILOT, V., LEFEVRE, J. C. & CHIESA, S. 2003. Comparative K-Ar and Ar/Ar dating of Ethiopian and Yemenite Oligocene volcanism: implications for timing and duration of the Ethiopian traps. *Earth and Planetary Science Letters*, **206**, 477–492.
- COURTILOT, V. E. 1980. Opening of the Gulf of Aden and Afar by progressive tearing. *Physics of Earth and Planetary Interiors*, **21**, 343–350.
- COURTILOT, V. E. 1982. Propagating rifts and continental breakup. *Tectonics*, **1**, 239–250.
- COURTILOT, V., JAUPART, C., MANIGHETTI, P., TAPPONNIER, P. & BESSE, J. 1999. On causal links between flood basalts and continental breakup. *Earth and Planetary Science Letters*, **166**, 177–195.
- CRANE, K. & BONATTI, E. 1987. The role of fracture zones during early Red Sea rifting: structural analysis using Space Shuttle radar and LANDSAT imagery. *Journal of the Geological Society, London*, **144**, 407–420.
- DAVISON, I., AL-KADASI, M. ET AL., 1994. Geological evolution of the southeastern Red Sea rift margin, Republic of Yemen. *Geological Society of America Bulletin*, **106**, 1474–1493.
- DEAN, S. M., MINSHULL, T. A., WHITMARSH, R. B. & LOUDEN, K. E. 2000. Deep structure of the ocean-continent transition on the southern Iberia Abyssal Plain from seismic refraction profiles: The IAM-9 transect at 40°20'N. *Journal of Geophysical Research*, **105**, 5859–5885.
- DEGENS, E. T. & ROSS, D. A. 1969. *Hot Brines and Recent Heavy Metal Deposits in the Red Sea*. Springer, Berlin.
- DIXON, T. H., STERN, R. J. & HUSSEIN, I. M. 1987. Control of Red Sea rift geometry by Precambrian structures. *Tectonics*, **6**, 551–572.
- DRURY, S. A., KELLEY, S. P., BEHRE, S. M., COLLIER, R. & ARAHA, M. Structures related to Red Sea evolution in northern Eritrea. *Tectonics*, **13**, 1371–1380.
- ELLIS, A. C., KERR, H. M., CORNWELL, C. P. & WILLIAMS, D. O. 1996. A tectono-stratigraphic framework for Yemen and its implications for hydrocarbon potential. *Petroleum Geoscience*, **2**, 29–42.
- EYAL, M., EYAL, Y., BARTOV, Y. & STEINITZ, G. 1981. The tectonic development of the western margin of the Gulf of Elat (Aqaba) Rift. *Tectonophysics*, **80**, 39–66.
- FERAUD, G., ZUMBO, V., SEBAI, A. & BERTRAND, H. 1991. $^{40}\text{Ar}/^{39}\text{Ar}$ Age and duration of tholeiitic magmatism related to the early opening of the Red Sea Rift. *Geophysical Research Letters*, **18**, 195–198.
- GARFUNKEL, Z., GINZBURG, A. & SEARLE, R. C. 1987. Fault pattern and mechanism of crustal separation along the axis of the Red Sea from side scan sonar (GLORIA) data. *Annales Geophysicae*, **5B**, 187–200.
- GAULIER, J. M., LEPICHON, X. ET AL. 1988a. Seismic study of the crustal thickness, Northern Red Sea and Gulf of Suez. *Tectonophysics*, **153**, 55–88.
- GAULIER, J. M., LEPICHON, X. ET AL. 1988b. Seismic study of the crust of the northern Red Sea and Gulf of Suez. *Tectonophysics*, **153**, 25–54.
- GETTINGS, M. E. 1982. Heat flow measurements at shot points along the 1978 Saudi Arabian deep-refraction line, Part II: Discussion and interpretation. US Geological Survey, Open File Report, **02-40**.
- GETTINGS, M. E. & SHOWAIL, A. 1982. Heat flow measurements at shot points along the 1978 Saudi Arabian deep-refraction line, Part I: Results and measurements. US Geological Survey, Open File Report, **02-39**.
- GETTINGS, M. E., BLANK, H. R., MOONEY, W. D. & HEALY, J. H. 1986. Crustal structure of southwestern Saudi Arabia. *Journal of Geophysical Research*, **91**, 6491–6512.
- GHEBREAB, W., CARTER, A., HURFORD, J. & TALBOT, C. J. 2002. Constraints for timing of extensional tectonics in the western margin of the Red Sea in Eritrea. *Earth and Planetary Science Letters*, **2000**, 107–119.
- GRANT, F. S. & WEST, G. F. 1965. *Interpretation Theory in Applied Geophysics*. McGraw-Hill, New York.
- GUENNOC, P., PAUTOT, G. & COUTELLE, A. 1988. Surface structures of the northern Red Sea axial valley from 23°N to 28°N: time and space evolution of neo-oceanic structures. *Tectonophysics*, **153**, 1–23.
- GUIRAUD, R. 1998. Mesozoic rifting and basin inversion along the northern Tethyan margin: an overview. In: MACGREGOR, D. S., MOODY, R. T. J. & CLARKLOWES, D. D. (eds) *Petroleum Geology of North Africa*. Geological Society, London, Special Publications, **132**, 217–229.
- GUIRAUD, R. & BOSWORTH, W. 1997. Senonian basin inversion and rejuvenation of rifting in Africa and Arabia: synthesis and implications to plate-scale tectonics. *Tectonophysics*, **282**, 39–82.

- GUIRAUD, R. & BOSWORTH, W. 1999. Phanerozoic geo-dynamic evolution of northeastern Africa and the northwestern Arabian platform. *Tectonophysics*, **315**, 73–108.
- GUIRAUD, R. & MAURIN, J. C. 1992. Early Cretaceous rifts of western and central Africa: an overview. *Tectonophysics*, **213**, 153–168.
- GUIRAUD, R., ISSAWI, B. & BOSWORTH, W. 2001. Phanerozoic history of Egypt and surrounding areas. In: ZIEGLER, P. A., CAVAZZA, W., ROBERTSON, A. H. F. & CRASQUIN-SOLEAU, S. (eds) *Peri-Tethys Memoir 6: Peri-Thetian Rift/Wrench Basins and Passive Margins*. Muséum national d'Histoire naturelle, Paris, 469–509.
- GUIRAUD, R., BOSWORTH, W., THIERRY, J. & DELPLANQUE, A. 2005. Phanerozoic geological evolution of Northern and Central Africa: An overview. *Journal of African Earth Sciences*, **43**, 83–143.
- HEALY, J. H., MOONEY, W. D., BLANK, H. R., GETTINGS, M. E., KOHLER, W. M., LAMSON, R. J. & LEONE, L. E. 1982. Saudi Arabian Seismic deep-refraction profile: final project report. US Geological Survey, Open File Report, **02-37**(IR-436).
- HOFMANN, C., COURTILOT, V., FERAUD, G., ROCHETTE, P., YIRGU, G., KETEFO, E. & PIK, R. 1997. Timing of the Ethiopian flood basalt event and implications for plume birth and global change. *Nature*, **389**, 838–841.
- HORSEFIELD, S. J., WHITMARSH, R. B., WHITE, R. S. & SIBUET, J. C. 1993. Crustal structure of the Goban Spur rifted continental margin, NE Atlantic. *Geophysical Journal International*, **119**, 1–19.
- IODP. 2001. Initial Science Plan 2003–2013; Earth, Oceans and Life, Scientific investigations of the Earth system using multiple drilling platforms and new technologies. Integrated Ocean Drilling Program. <http://www.iodp.org/isp/>, 2001.
- IZZELDIN, A. Y. 1987. Seismic, gravity and magnetic surveys in the central part of the Red Sea: their interpretation and implications for the structure and evolution of the Red Sea. *Tectonophysics*, **143**, 269–306.
- JESTIN, F., HUCHON, P. & GAULIER, J. M. 1994. The Somalia plate and the East African Rift System: present-day kinematics. *Geophysical Journal International*, **116**, 637–654.
- JOFFE, S. & GARFUNKEL, Z. 1987. Plate kinematics of the circum Red Sea—A re-evaluation. *Tectonophysics*, **141**, 5–23.
- KARNER, G. D. 2005. Structural and depositional styles of the syn-rift systems of the West African and Brazilian margins: The need for new quantitative approaches for modeling basin subsidence. (Abstract) In: *Return to Rifts—The Next Wave? Fresh Insights into the Petroleum Geology of Global Rift Basins*, 5–7 April. Geological Society, London, 18–19.
- KARNER, G., DRISCOLL, N. W. & BARKER, D. H. N. 2003. Syn-rift regional subsidence across the West African continental margin: the role of lower plate ductile extension. In: ARTHUR, T. J., MACGREGOR, D. S. & CAMERON, N. R. (eds) *Petroleum Geology of Africa: New Themes and Developing Technologies*. Geological Society, London, Special Publications, **207**, 105–129.
- KENE, N. H., EBINGER, C. J. & REX, D. C. 2001. Late Oligocene volcanism and extension in the southern Red Sea Hills, Sudan. *Journal of the Geological Society, London*, **158**, 285–294.
- KLITGORD, K. D. & BEHRENDT, J. C. 1979. Basin structure of the U.S. Atlantic margin. In: WATKINS, J. S., MONTADERT, L. & DICKERSON, P. W. (eds) *Geological and Geophysical Investigation of Continental Margins*. American Association of Petroleum Geologists Memoir, **29**, Tulsa, OK, 85–112.
- KNOPOFF, L. & FOUDA, A. A. 1975. Upper-mantle structure beneath the Arabian Peninsula. *Tectonophysics*, **26**, 121–134.
- KNOTT, S. T., BUNCE, E. T. & CHASE, R. L. 1966. Red Sea Seismic Reflection Studies. In *The World Rift System*. Geological Survey of Canada, Paper, **66-14**, 78–97.
- KRÖNER, A., LINNEBACHER, P., STERN, R. J., REISCHMANN, T., MANTON, W. & HUSSEIN, I. M. 1991. Evolution of Pan-African island arc assemblages in the southern Red Sea Hills, Sudan, and in southwestern Arabia as exemplified by geochemistry and geochronology. *Precambrian Research*, **53**, 99–118.
- MAKRIS, J., STOEFEN, B., VEES, R., ALLEM, A., MAAMOUN, M. & SHEHATA, W. 1979. *Deep seismic soundings in Egypt: Part II: Crust and upper mantle of the Red Sea Coast*. University of Hamburg, Internal Report.
- MAKRIS, J., ALLAM, A., MOKTAR, T., BASAHEL, A., DEHGHANI, G. A. & BAZARI, M. 1983. Crustal structure in the northwestern region of the Arabian Shield and its transition to the Red Sea. *Bulletin of the Faculty of Science of King Abdulaziz University*, **6**, 435–447.
- MARTINEZ, F. & COCHRAN, J. R. 1988. Structure and tectonics of the northern Red Sea: Catching a continental margin between rifting and drifting. *Tectonophysics*, **150**, 1–32.
- MARTINEZ, F. & COCHRAN, J. R. 1989. Geothermal measurements in the northern Red sea: Implications for lithospheric thermal structure and mode of extension during continental rifting. *Journal of Geophysical Research*, **94**, 12,239–12,266.
- MAURY, R. C., BOUGAULT, H., COUTELLE, A., GUENNOC, P., JORON, J.-L. & PAUTOT, G. 1985. Présence de ferrobasalte tholéïtique dans la fosse Jean-Charcot ($26^{\circ}15'N$, $35^{\circ}22'E$): signification dans le contexte géodynamique du Mer Rouge. *Comptes Rendus de l'Academie des Sciences Paris*, **300**, 811–817.
- MILLER, S. P., MACDONALD, K. C. & LONSDALE, P. 1985. Near bottom magnetic profile across the Red Sea. *Marine Geophysical Researches*, **7**, 401–418.
- MOHR, P. A. 1983. Ethiopian flood basalt province. *Nature*, **303**, 577–584.
- MONTENTAT, C., OTT D'ESTEVOU, P. ET AL. 1988. Tectonic and sedimentary evolution of the Gulf of Suez and the northwestern Red Sea. *Tectonophysics*, **153**, 161–177.
- MORGAN, P., BOULOS, F. F., HENNIN, S. F., EL-SHERIFF, A. A., EL-SAYED, A. A., BASTA, N. Z. & MELEK, Y. S. 1985. Heat flow in eastern Egypt: The thermal signature of a continental breakup. *Journal of Geodynamics*, **4**, 107–131.

- MOUSTAFA, A. R. & KHALIL, M. H. 1990. Structural characteristics and tectonic evolution of north Sinai fold belts. In: SAID, R. (ed.) *The Geology of Egypt*. A.A. Balkema, Rotterdam, 381–389.
- MOUSTAFA, A. R. & KHALIL, M. H. 1994. Rejuvenation of the eastern Mediterranean passive continental margin in northern and central Sinai: new data from the Themed Fault. *Geological Magazine*, **131**, 435–448.
- OMAR, G. I. & STECKLER, M. S. 1995. Fission track evidence on the initial rifting of the Red Sea: two pulses, no propagation. *Science*, **270**, 1341–1344.
- OMAR, G. I., STECKLER, M. S., BUCK, W. R. & KOHN, B. P. 1989. Fission-track analysis of basement apatites at the western margin of the Gulf of Suez rift, Egypt: evidence for synchronicity of uplift and subsidence. *Earth and Planetary Science Letters*, **94**, 316–328.
- PALLISTER, J. S. 1987. Magmatic history of Red Sea rifting: Perspective from the central Saudi Arabian coastal plain. *Bulletin of the Geological Society of America*, **98**, 400–417.
- PARKER, R. L. 1973. The rapid calculation of potential anomalies. *Geophysical Journal of the Royal Astronomical Society*, **31**, 447–455, 1973.
- PATTON, T. L., MOUSTAFA, A. R., NELSON, R. A. & ABDINE, A. S. 1994. Tectonic evolution and structural setting of the Suez Rift. In: LANDON, S. M. (ed.) *Interior Rift Basins*. AAPG, Tulsa, OK, 9–55.
- PAUTOT, G. 1983. Les fosses de la Mer Rouge: approche geomorphologique d'un stade initial d'ouverture oceانية réalisée à l'aide du Seabeam. *Oceanologica Acta*, **6**, 235–244.
- PAUTOT, G., GUENNO, P., COUTELLE, A. & LYBERIS, N. 1984. Discovery of a large brine deep in the northern Red Sea. *Nature*, **310**, 133–136.
- PAUTOT, G., GUENNO, P., COUTELLE, A. & LYBERIS, N. 1986. La dépression axiale du segment nord Mer Rouge (de 25°N à 28°N): Nouvelles données géologiques et géophysiques obtenues au cours de la campagne TRANSMEROU 83. *Bulletin de la Société Géologique de France*, **8**, 381–399.
- PEDDY, C., PINET, B. ET AL. 1989. Crustal structure of the Goban spur continental margin, Northeast Atlantic, from deep seismic reflection profiling. *Journal of Geological Society, London*, **146**, 427–437.
- PICKUP, S. L. B., WHITMARSH, R. B., FOWLER, C. M. R. & RESTON, T. J. 1996. Insight into the nature of the ocean-continent transition off West Iberia from a deep multichannel seismic reflection profile. *Geology*, **24**, 1079–1082.
- PURSER, B. H. & HÖTZL, H. 1988. The sedimentary evolution of the Red Sea rift: a comparison of the northwest (Egyptian) and northeast (Saudi Arabian) margins. *Tectonophysics*, **153**, 193–208.
- REDFERN, P. & JONES, J. A. 1995. The interior rifts of Yemen – analysis of basin structure and stratigraphy in a regional plate tectonic context. *Basin Research*, **7**, 337–356.
- RICHARDS, M. A., DUNCAN, R. A. & COURTILOT, V. 1989. Flood basalts and hot-spot tracks: Plume heads and tails. *Science*, **246**, 103–107.
- RIHM, R., MAKRIS, J. & MÖLLER, L. 1991. Seismic surveys in the Northern Red Sea: asymmetric crustal structure. *Tectonophysics*, **198**, 279–295.
- ROESER, H. A. 1975. A detailed magnetic survey of the southern Red Sea. *Geologische Jahrbuch*, **13**, 131–153.
- SALAH, M. G. & AL SHARHAN, A. S. 1996. Structural influence on hydrocarbon entrapment in the northwestern Red Sea. *AAPG Bulletin*, **80**, 101–118.
- SEBAI, A., ZUMBO, V., FERAUD, G., BERTRAND, H., HUSSAIN, A. G., GIANNERIN, G. & CAMPREDON, R. 1991. $^{40}\text{Ar}/^{39}\text{Ar}$ dating of alkaline and tholeiitic magmatism of Saudi Arabia related to the early Red Sea rifting. *Earth and Planetary Science Letters*, **104**, 473–487.
- SMITH, W. H. F. & SANDWELL, D. T. 1997. Global sea floor topography from satellite altimetry and ship depth soundings. *Science*, **277**, 1956–1962.
- STECKLER, M. S. & TEN BRINK, U. S. 1986. Lithospheric strength variations as a control on new plate boundaries: examples from the northern Red Sea region. *Earth and Planetary Science Letters*, **79**, 120–132.
- STOESER, D. B. & CAMP, V. E. 1985. Pan-African microplate accretion of the Arabian Shield. *Geological Society America Bulletin*, **96**, 817–826.
- UKSTINS, I. A., RENNE, P. R., WOLFENDEN, E., BAKER, J., AYALEW, D. & MENZIES, M. A. 2002. Matching conjugate volcanic margins: $^{40}\text{Ar}/^{39}\text{Ar}$ chronostratigraphy of pre- and syn-rift bimodal flood volcanism in Ethiopia and Yemen. *Earth and Planetary Science Letters*, **198**, 289–306.
- VAIL, J. R. 1985. Pan-African (late Precambrian) tectonic terrains and the reconstruction of the Arabian-Nubian shield. *Geology*, **13**, 839–842.
- WERNER, S. 1953. Interpretation of aeromagnetic anomalies as sheet-like bodies, *Sveriges Geologista Undersök Series C, Arsbok*, **43**, N: 06, Stockholm, Sweden.
- WESSEL, P. & SMITH, W. H. F. 1998. New improved version of Generic Mapping Tools released. *Eos, Transactions of the American Geophysical Union*, **79**, 579.
- WHITMARSH, R. B., MANATSCHAL, G. & MINSHULL, T. A. 2001. Evolution of magma-poor continental margins from rifting to seafloor spreading. *Nature*, **413**, 150–154.
- ZUMBO, V., FERAUD, G., BERTRAND, H. & CHAZOT, G. 1995a. $^{40}\text{Ar}/^{39}\text{Ar}$ chronology of tertiary magmatic activity in southern Yemen during the early Red Sea–Aden rifting. *Journal of Volcanology and Geothermal Research*, **65**, 265–279.
- ZUMBO, V., FERAUD, G., VELLUTINI, P., PIGUET, P. & VINCENT, J. 1995b. First $^{40}\text{Ar}/^{39}\text{Ar}$ dating on early Pliocene to Plio-Pleistocene magmatic events of the Afar–Republic of Djibouti. *Journal of Volcanology and Geothermal Research*, **65**, 281–295.

